Size Optimization of Utility-Scale Solar PV System Considering Reliability Evaluation

By

Xiao Chen

Thesis submitted to the faculty of the
Virginia Polytechnic Institute and State University
In partial fulfillment of the requirements for the degree of

Master of Science
In
Electrical Engineering

Virgilio A. Centeno, Chair
Jaime De La Ree Lopez
Vassilis Kekatos

June 14, 2016
Blacksburg, Virginia

Keywords: Sizing optimization; Photovoltaics; Reliability evaluation

Size Optimization of Utility-Scale Solar System Considering Reliability Evaluation

Xiao Chen

ABSTRACT

In this work, a size optimization approach for utility-scale solar photovoltaic (PV) systems is proposed. The purpose of the method is to determine the optimal solar energy generation capacity and optimal location by the minimizing total system cost subject to the constraint that the system reliability requirements. Due to the stochastic characteristic of the solar irradiation, the reliability performance of a power system with PV generation is quite different from the one with only conventional generation. Basically, generation adequacy level of power systems containing solar energy is evaluated by reliability assessment and the most widely used reliability index is the loss of load probability (LOLP). The value of LOLP depends on various factors such as power output of the PV system, outage rate of generating facilities and the system load profile. To obtain the LOLP, the Monte Carlo method is applied to simulate the reliability performance of the solar penetrated power system. The total system cost model consists of the system installation cost, mitigation cost, and saving fuel & operation cost. Mitigation cost is accomplished with N-1 contingency analysis. The cost function minimization process is implemented in Genetic Algorithm toolbox, which has the ability to search the global optimum with relative computational simplicity.

Acknowledgements

The presented work is benefited from Chetan Mishra, who is always willing to help whenever I ran into a trouble about my research, Elliott J. Mitchell-Clogan, who provide support on programing in Loss of Load Probability Evaluation , the National Renewable Energy Labs (NREL), who made the National Solar Radiation Data publicly available, the MATPOWER team, who provide excellent simple Newton-Raphson Power Flow solution, and the IEEE and members who made Roy Billinton Reliability Test System and data available.

I would also like to thank Dr. Virgilio Centeno, Dr. Jaime De La Ree Lopez, Dr. Vassilis Kekatos, and other professors of Virginia Tech from whom I have learnt a lot during my time studying here. I feel greatly inspired to chat with professors, students in our lab, and people around me and benefit a lot from their thoughts and comments.

Finally, I must express my very profound gratitude to my parents and my family for providing me with unfailing support and continuous encouragement throughout my years of study and through the process of researching.

This accomplishment would not have been possible without all of you. Thank you.

Table of Contents

List of Figures

List of Table

Nomenclature

A_{pv}	Covering land area of the PV panels (m^2)
C_{pv}	PV system generation capacity (W)
C_{pv_min}	Minimum permissible PV system capacity (W)
C_{pv_max}	Maximum permissible PV system capacity (W)
c_{pv}	PV cost per unit ($/W)
C_C	Capital installation cost ($)
C_m	Mitigation cost ($)
C_s	Saving operation cost ($)
C_{line}	Unit cost of line in ($)
C_{SVC}	Unit cost of SVC in ($/MVAR)
L_{line}	Length of transmission line (mile)
Q	Reactive power capacity (MVAr)
E_{pv}	Hourly PV energy production (W)
E_{sun}	Hourly solar irradiation in (W/m^2)
L_y	Annual peak load (W)
$L(t)$	Hourly load demand of the system (W)
P_g	Total available generation capacity (W)
P_w	Percentage of weekly load in terms of the annual peak
P_d	Percentage of daily load in terms of the weekly peak
$P_h(t)$	Percentage of hourly load in terms of daily peak.
η_{pv}	Efficiency of PV module
η_{inv}	Efficiency of inverter
η_{wir}	Efficiency of wires
V_{goal}	Desired operation bus voltage (p.u.)
Y_{ij}	Mutual admittance between nodes i and j
$\widetilde{V}_i$	Phasor voltage to ground at node i
$\widetilde{I}_i$	Phasor current flowing into the network at node i

Acronyms

AC	Alternate Current
CDF	Cumulative Density Function
CSP	Concentrating Solar Power
DC	Direct Current
ED	Energy Deficit
ENS	Energy Not Supplied
LLD	Loss of Load Duration
LOLP	Loss of Load Probability
FOR	Forced Outage Rate
MCS	Monte Carlo Simulation
MTTF	Mean Time to Failure
MTTR	Mean Time to Repair
NREL	National Renewable Energy Laboratory
PDF	Probability density function
PV	Photovoltaic
RTS	Reliability Test System
SMT	Scheduled maintenance time
SVC	Static Var Compensator
TMY	Typical Meteorological Year
TTF	Time to Fail
TTR	Time to Repair

Chapter 1
Introduction

For many years, consumers' electric energy demand has been increasing, so has done the generation capacity of power plants. Among multiple energy supplying methods, solar photovoltaic (PV) is widely used as renewable source to provide electricity power to consumers. Solar PV can convert free and unlimited sunlight to electricity without carbon dioxide emission or any other air pollutants. Given these advantages, large-scale solar PV generation has been gradually integrated into power grids to serve energy need. When the utility company plans to install solar PV generation in their system, both installation capacity and location of PV are the main concerns. Due to the uncertain characteristics of sunlight, the solar penetration level in a system is usually limited by some reliability constraints. In this research, the system performance of PV penetration at specific location is simulated by Monte Carlo simulation and the probability of contingency consequences are forecasted through contingency analysis. When designing the optimal PV size in a system with minimum cost, the result of the system reliability evaluation can be directly used as the optimization constraint in order to meet system reliability requirements.

In this chapter, the development of solar energy generation in past years is discussed. The motivation and objective of this research and the outline of this thesis is presented at the end of the chapter.

1.1 Background of Power System

The primary function of electric power system is to provide electric energy to its customers with an acceptable degree of continuity and quality. Electric power is generated in the power plant. High-voltage transmission line connected with power plant can transmit the electric power to residential area. And the power is adjusted by power substation and transmission lines which step down the voltage and distribute to the industrial, commercial and residential loads.

Today transmission lines carry high-voltage three-phase alternating current (AC). The transmission line separates the system into two parts: generation and distribution system. A simple diagram of an electricity grid is shown in Figure 1-1. Red, blue, green are noted to distinguish the generation, transmission and distribution sections correspondingly. At the generating system, electricity is generated and the voltage is stepped up for transition at high voltages (115 kV or above) in order to reduce power loss over the long-distance transmission. In the distribution network, voltage is stepped down below 33 kV to serve the customer energy demand.

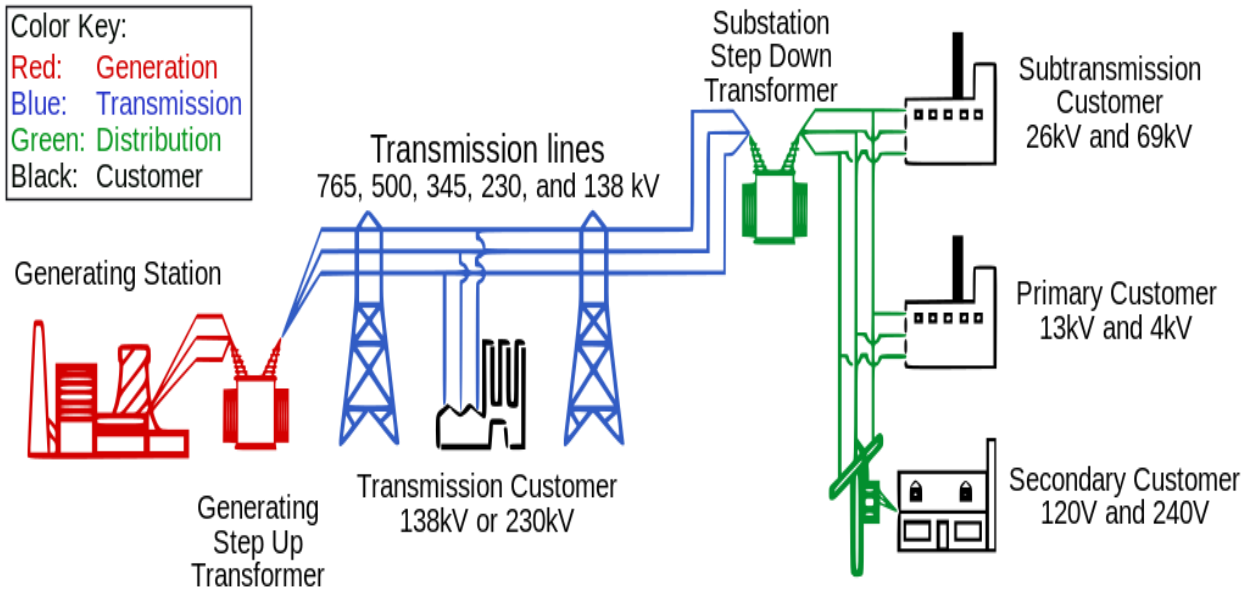

Figure 1. Diagram of an electric power system *[1]*

Most conventional power plants use fossil fuel as energy source to generate electricity. Three essential fossil fuels in US are coal, petroleum and natural gas. Two-thirds of these fuel energy gets lost as heat during electricity production. Additionally, the combustion of fossil-fuel also emits large amounts of carbon dioxide (CO_2), which is the primary greenhouse gas [2]. Traditional power generation method of utilizing nonrenewable fuel is a principal factor for the rapid augmentation of global greenhouse gas emission. Figure 1-2 depicts the U.S. carbon dioxide emission by source. It shows that fossil fuel burned for electricity is responsible for about 37% of U.S. CO_2 emission [3]. The cost of laboring coal mines, drilling oil plants and that of transporting fuel to the plants can be covered by electricity bills. However, some other costs of using fossil fuel are paid by the suffering of the entire society. These include air pollution, damage to land and soil, health threats to miners, global warming, and acid rain [2, 3].

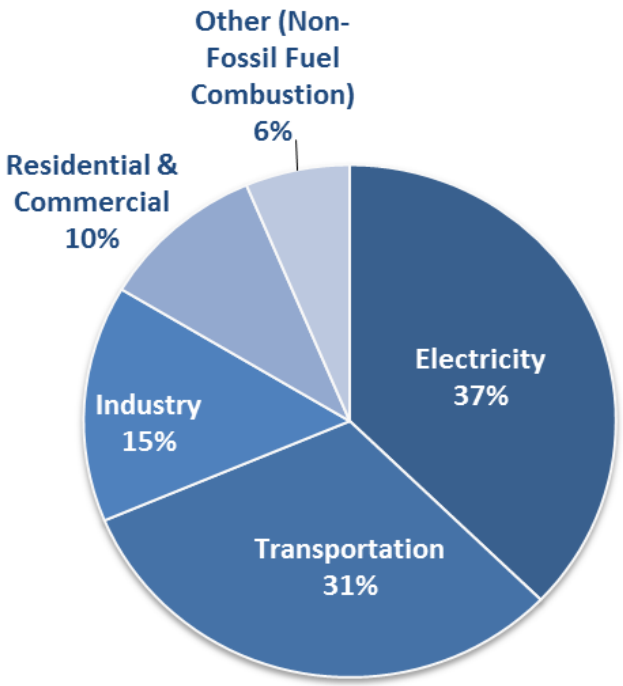

Figure 2. U.S. Carbon dioxide emission by source *[3]*

As the electricity consumption grows every year, utility companies keep adding more generation capacity in the system. However, increasing capacity of traditional power plants in the system incurs the environmental problems aforementioned. To reduce the environmental deterioration due to fossil fuel combustion, utility companies have been seeking opportunities to take more advantage of renewable energy sources for power generation in recent decades.

Thanks to the development of renewable energy generation technology, electricity generation with new energy source has already been integrated in our system. Table 1-1 shows the tendency of percentage changes of electricity generating capacity by different sources since 2004. It illustrates that the renewable energy sources is accounted for about 9.4% of total U.S. energy generation in 2004 and grew up to about 15.5% by 2014 [4]. Although fossil fuel, especially coal and natural gas, still dominate the energy sources, renewable sources are expected to gradually elevate our independences on fossil fuel and part of traditional generating facilities will be substituted by renewable generation technologies in the near future.

Table 1-1. U.S. Electricity Generation Capacity by Sources *[4]*

	Coal	Petroleum	Natural Gas	Other Gases	Nuclear	Renewables[1]	Other	Total Capacity (MW)
2004	32.5%	6.3%	41.0%	0.2%	10.2%	9.6%	0.1%	1,030,025
2005	32.1%	6.2%	41.7%	0.2%	10.1%	9.7%	0.1%	1,047,655
2006	31.8%	6.1%	41.9%	0.2%	10.0%	9.9%	0.1%	1,056,216
2007	31.5%	5.8%	42.1%	0.2%	9.9%	10.3%	0.1%	1,066,842
2008	30.5%	5.6%	41.4%	0.2%	9.6%	11.1%	0.1%	1,082,975
2009	30.7%	5.7%	41.7%	0.2%	9.7%	11.9%	0.1%	1,101,987
2010	30.6%	5.6%	41.7%	0.3%	9.5%	12.2%	0.1%	1,119,603
2011	30.3%	5.1%	42.1%	0.2%	9.4%	12.8%	0.1%	1,134,997
2012	29.2%	4.7%	42.3%	0.2%	9.4%	14.1%	0.1%	1,150,110
2013	28.8%	4.5%	42.6%	0.3%	9.0%	14.6%	0.1%	1,152,303
2014	28.1%	4.2%	42.8%	0.3%	9.0%	15.5%	0.1%	1,158,416

1.2 Photovoltaic Generation

Solar photovoltaic plays an important role in renewable energy generation because it can bring great benefits to both utility companies and electricity consumers like [5]:

- Reduce the risk of fuel-price volatility,
- Reduce CO_2 emissions and improve air quality,
- Operate quietly and fewer maintenance for long period,
- Provide peaking generation to meet the growing energy demand,
- Reduce generator operating time and increase operational life.

With all those advantages, solar PV generation represents an economical and attractive option for electric power system which mainly depends on fossil fuel.

According to the 2014 Renewable Energy Data Book from the National Renewable Energy Laboratory (NREL), solar PV and concentrating solar power (CSP) have continued to be one of the most rapidly growing renewable electricity technologies [4]. The continuing enhancements in

PV system inverter technology drives the increasing demand of grid-connected solar PV electricity in power system. Table 1-2 shows a solar PV electricity installed capacity increase of more than 50% (6 GW), and a CSP significantly increase of more than 80% from 2013 to 2014 [4]. Solar PV energy is possibly the most common generation type in power systems.

Table 1-2. Cumulative U.S. Renewable Electricity Capacity (MW) and Annual Percent Change *[4]*

	Hydropower	Solar PV[1]	CSP	Wind	Geothermal[2]	Biomass	Total Renewables[3]
2004	77,130 (0.1%)	161 (56.3%)	354 (0%)	6,725 (5.9%)	2,798 (0%)	11,033 (1.6%)	98,164 (0.7%)
2005	77,354 (0.3%)	240 (49.1%)	354 (0%)	9,121 (35.6%)	2,828 (1.1%)	11,222 (1.7%)	101,064 (3.0%)
2006	77,419 (0.1%)	345 (43.8%)	355 (0.3%)	11,575 (26.9%)	2,831 (1.7%)	11,553 (2.9%)	103,999 (2.9%)
2007	77,432 (0%)	505 (46.4%)	419 (18%)	16,812 (45.2%)	2,936 (2.0%)	11,738 (1.6%)	109,726 (5.5%)
2008	77,640 (0.3%)	803 (59%)	419 (0%)	25,237 (50.1%)	3,039 (1.4%)	12,485 (6.4%)	119,438 (8.9%)
2009	77,910 (0.3%)	1,185 (47.6%)	430 (2.6%)	35,155 (39.3%)	3,085 (3.5%)	12,836 (2.8%)	130,329 (9.1%)
2010	78,204 (0.4%)	2,037 (71.9%)	508 (18.1%)	40,267 (14.5%)	3,100 (2.3%)	13,053 (1.7%)	136,701 (4.9%)
2011	78,194 (0%)	3,959 (94.4%)	508 (0%)	46,916 (16.5%)	3,238 (0.1%)	13,207 (1.2%)	145,111 (6.2%)
2012	78,241 (0.1%)	7,328 (85.1%)	508 (0%)	60,005 (27.9%)	3,385 (6.4%)	14,047 (6.4%)	161,829 (11.5%)
2013	78,457 (0.3%)	12,140 (65.2%)	918 (80.7%)	61,107 (1.8%)	3,792 (1.0%)	14,705 (4.7%)	168,299 (4.0%)
2014	78,809 (0.4%)	18,305 (51.2%)	1,685 (83.6%)	65,879 (7.8%)	3,789 (0.7%)	15,408 (4.8%)	179,665 (6.8%)

Unlike any power generation technology, solar PV power systems are essentially electric power generation devices that absorb the sun's emanated energy in the form of photons and convert them into electric power. Simply stated, solar power cells will produce electrical energy when the sun sheds lights on the surface of PV cells [6]. As we all know, the sun rises in the morning from the east and sets in the west. Therefore, solar photovoltaic power modules produce electrical energy only during daylight hours. Figure 1-3 depicts a daily solar power energy production curve. In a solar PV system, the amount of power harvested from the sun is directly proportional to the radiation amount of sunlight. Technically, the maximum power output of solar PV system happens in exactly the same hours that solar panels have the most intensive solar exposure [6].

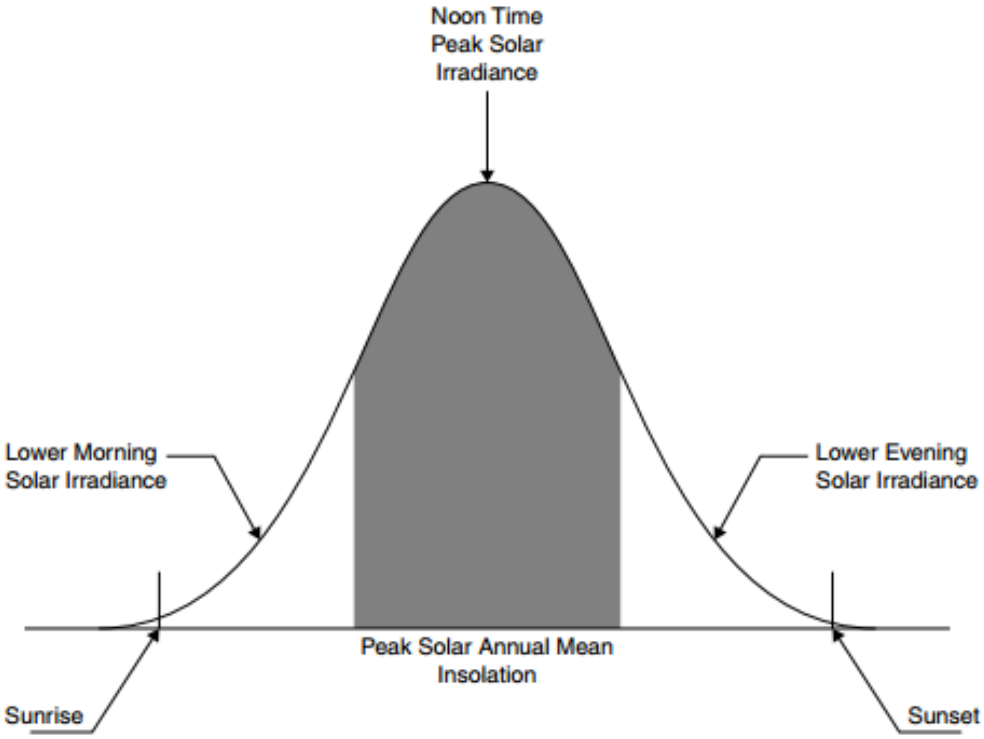

Figure 3. Daily solar power energy production curve *[6]*

For a solar PV generating unit, the PV cell is the most fundamental component. PV cells are connected in parallel to increase the current and in series to obtain a larger voltage and that composes a PV module. A PV panel is assembled with one or many numbers of PV modules while a PV array is constituted from a number of PV panels, and used as a complete power-generating unit. In general, solar power modules have a 25 years' warranty.

Figure 1-4 is a grid connected solar PV system diagram. In a grid connected solar PV system, PV modules convert solar irradiation to DC electric power and are wired to the power conditioner. The power conditioner is an electronic device that converts DC power to commercial AC power and protects the grid interconnection. Step-up transformer connects the output power from the power conditioner to the utility company grid. Switch gear controls the link between solar PV generation system and the utility grid [7].

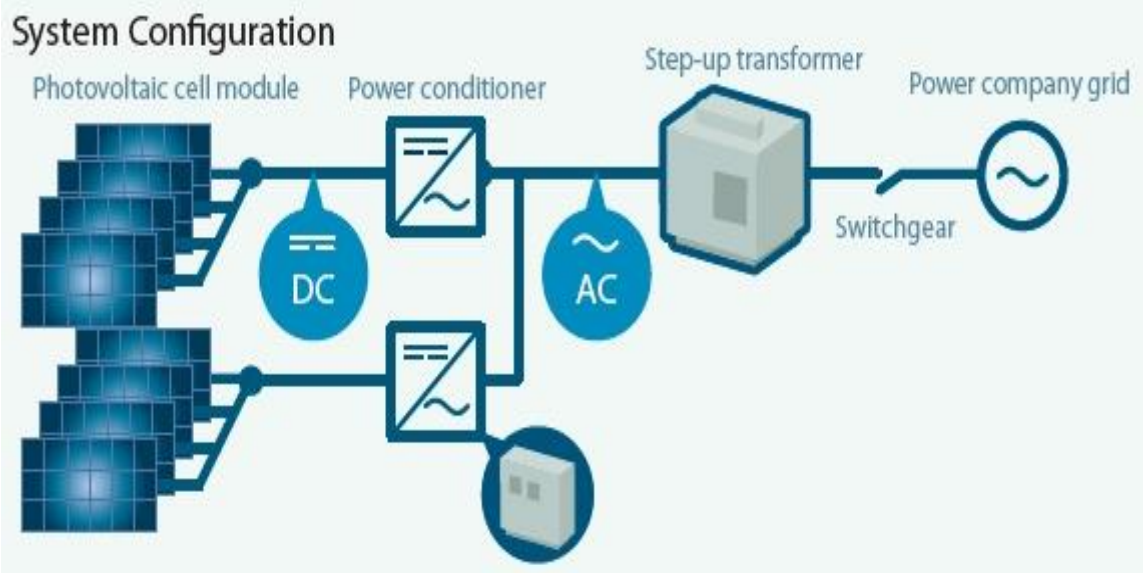

Figure 4. Grid connected solar PV system diagram *[7]*

By generating clean energy without any air pollution, solar PV generation can help balance the environmental protection with the electricity energy demands. Utility companies tend to design and operate large-scale solar PV systems to replace more conventional generating units. According to the Solar Energy Industries Association, utility-scale solar system is defined as the size of PV generation system that is greater than 1-MW. Figure 1-5 shows the 20-MW Remington Solar Power Facility built by Dominion Virginia Power. Remington Solar would be Virginia's first large scale solar facility, which is constructed from approximately 90,000 photovoltaic panels on approximately 125 acres of land [8].

Figure 5. Virginia Solar Project in Fauquier County *[8]*

Even though solar PV technologies have made huge technological and cost improvements, solar electricity still has a higher cost compared with regular electricity. Additionally, the location of solar PV panels must be carefully planned. Cities which are covered by landscapes and trees and surrounded by high buildings may not be desirable enough for installing the large-scale solar PV system. Areas that remain cloudy most of the day will reduce efficiency of PV modules. Furthermore, the energy output will not be as stable as that of the conventional generating unit because solar irradiation is subjected to varying with weather and time conditions. Consequently, the reliability level could be a problem due to generation insufficiency.

With regard to the reliability level of power system, the capacity of solar PV system must be adjusted to get the most economical configuration while satisfying the system reliable operation requirements.

1.3 Research Objective and Approach

The growing penetrations of solar PV energy creates challenges to grid reliability, operations and compatibility with the existing system. This research addresses the power system reliability evaluation, economic benefits and security problem to determine the optimal size of a solar PV system. The proposed method is simulated on the IEEE 24-bus Reliability Test System (RTS) in MATLAB. This test system is provided with detail information of generating units, buses and branches in the MATPOWER case file. The model provides the reliability data of each generator.

To find out the optimal capacity of the solar PV system in RTS, an optimization problem is developed with a target function and variable constraints. As for the constraint, the possibility of incurring loss of load due to generation inadequacy is evaluated to guarantee system stability and reliability performance. The target function is the economic cost of solar PV system. This cost function takes into account the operation cost that protecting and assisting the system from all possible system contingencies. Accounting for these considerations, the optimization problem is formulated in a three steps process:

1. Loss of load probability evaluation of electric power system,
2. Contingency violation cost assessment with solar PV placement,
3. Size optimization based on total cost of solar PV system.

To be more specific, cost estimation of solar PV system consists of fixed installation cost and mitigation cost. Fixed cost is proportional to the size of solar PV. Meanwhile, mitigation cost integrates the line overload cost and bus voltage collapse cost in all system contingencies. Newton-Raphson power flow method is applied to find out the system operating condition in N-1 contingency analysis. Branch overload violation and bus voltage collapse are examined by power flow results after taking one line out of service. The solution of the optimization problem is limited by the generation adequacy constraints -- Loss of Load Probability (LOLP), which is calculated with State Duration Sampling Method and validated using Monte Carlo simulation.

1.4 Thesis Organization

This thesis consists of seven chapters including the research background and objectives stated in Chapter 1. Chapter 2 outlines necessary power system modeling and analysis skills. Newton-Raphson method is detailed and the MATPOWER toolbox is briefly introduced. N-1 contingency analysis is also examined to find out the potential operation risks of the system in Chapter 3. System reliability evaluation of electric power system is described in Chapter 4. Monte Carlo Simulation is utilized to validate the LOLP results of the system. The system cost function is modeled and optimized in Chapter 5. The computational heuristic optimization process is accomplished with the genetic algorithm toolbox in MATLAB. Chapter 6 illustrates the simulation results and analyzes the optimization results with different PV displacement ratio and location placement. Finally, Chapter 7 provides the conclusions and future research interests.

Chapter 2
Power Flow Analysis

Power flow analysis is an essential analysis tool for power engineers to find the steady-state operating point of an electric power system. Technically, given the load demanded at consumption buses and the power supplied by generators, this analysis can solve all bus voltages, (both magnitudes and angles) and all real and reactive power injections on each bus of the system. The system is assumed to be balanced and this enables a single-phase representation of the power system.

This chapter is focused on the basic characteristics of the AC power flow applied to the steady-state performance of the power system. The modeling of system network is described on the basis of transmission line model and the basic network equations are presented here. To obtain the network equation solution, Newton-Raphson power flow method is introduced in detail. And at the end of this chapter, an overview of power flow computation with the utilization of MATPOWER is included.

2.1 Modeling of Transmission Line

In an electric power system, overhead transmission lines are used for long distances 3-phase electricity transmission. A transmission line is characterized by four parameters, which are briefly defined in [9]:

a) *Series Resistance (R).* The resistances of lines are determined by resistivity and the skin effect of conductor.
b) *Shunt Conductance (G).* The shunt conductance is due to the effect of leakage currents along power lines. In transmission system, the leakage current effect is relatively small and normally negligible for practical purpose.

c) *Series Inductance (L).* The series inductance is produced by the magnetic flux linkages surrounding the conductor cross area and those between each phase of the lines. For practical reason, the inductances of the three phases with non-equilateral spacing can be equalized by transposing the lines.

d) *Shunt Capacitance (C).* The line capacitance represents the charging phenomenon between conductors due to potential differences between power lines. When alternating voltages are applied to the power lines, a charging current flows caused by alternate charging and discharging of the capacitances.

It should be noted that if three-phase lines are placed in transposed configuration, they can be represented by a single phase model. Thus the relationship between current and voltage can be expressed in terms of one phase of the line:

$$Z = R + j\omega L \qquad (2\text{-}1)$$

$$Y = G + j\omega C \qquad (2\text{-}2)$$

or

$$Z = R + jX \qquad (2\text{-}3)$$

$$Y = G + jB \qquad (2\text{-}4)$$

As in the real case, overhead lines are generally categorized into three classes based on their length [9]:

a) *Short lines*: lines with the length less than 80 km (50 mi). Their shunt capacitances are neglected and may be represented by their series impedance.

b) *Medium-length lines*: lines with the length over 80 km (50 mi) but less than 200km (150 mi), may be represented by the nominal π equivalent model.

c) *Long lines*: lines longer than 200 km. Such lines can be represented by the nominal π equivalent model.

The parameters of the medium-length overhead lines are significantly influenced by its distributed effects and Table 2-1 gives the typical parameters of overhead transmission line with nominal voltage varying from 230 kV to 1,100 kV [9].

Table 2-1. Typical Overhead Transmission Line Parameters *[9]*

Nominal Voltage	**230 kV**	**345 kV**	**500 kV**	**765 kV**	**1,100 kV**
R (Ω/km)	0.050	0.037	0.028	0.012	0.005
$x_L = \omega L$ (Ω/km)	0.488	0.367	0.325	0.329	0.292
$b_c = \omega C$ (μs/km)	3.371	4.518	5.200	4.978	5.544

Notes: 1. Rated frequency is assumed to be 60 Hz.

2. Bundled conductors used for all lines listed, except for the 230 kV lines.

3. R, x_L, and b_c are per-phase values.

In transmission systems, overhead lines of 160 km length and of any voltage rating are practically represented by the nominal π equivalent model as shown in Figure 2-1.

The shunt admittance Y and series impedance Z are noted for the whole line, single-phase. With this equivalent circuit, given the complex voltages of the terminal buses, sending and receiving power flows and power losses can be obtained.

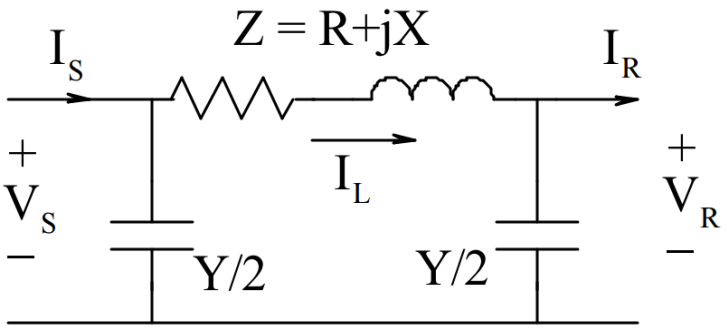

Figure 6. Pi equivalent circuit for an overhead transmission line

The current flowing through the line is

$$I_L = I_S - \frac{Y}{2}V_S \qquad (2\text{-}5)$$

The current at the receiving ending is

$$I_R = I_L + \frac{Y}{2}V_R \qquad (2\text{-}6)$$

The voltage at the sending end is given by

$$V_S = V_R + ZI_L \qquad (2\text{-}7)$$

Apparent power transferred from sending terminal is

$$S_S = V_S I_S \qquad (2\text{-}8)$$

Power injected to the receiving terminal is

$$S_R = V_R I_R \qquad (2\text{-}9)$$

Considering the losses due to shunt admittance of the line $Y/2$ seeing from the sending end, apparent power flow on line is essentially represented by

$$S_L = \mathrm{V}_S I_S - \frac{Y}{2}\mathrm{V}_S{}^2 \qquad (2\text{-}10)$$

or

$$S_L = S_S - \frac{Y}{2}\mathrm{V}_S{}^2 \qquad (2\text{-}11)$$

Since the shunt conductance G due to leakage currents is very small compared to line currents, it is practically neglected in transmission system. Equation 2-11 then reduces to

$$S_L = S_S - \frac{B}{2}\mathrm{V}_S{}^2 \qquad (2\text{-}12)$$

2.2 Network Equations Formulation

The power flow analysis consists of the calculation of power flows and voltages of a transmission network with specified bus and generator information. The basic requirement of the system is to be balanced and then the power flow analysis can be applied to simulate the steady-state operation [9].

There are four quantities taken into account to define each bus: active power P, reactive power Q, voltage magnitude V, and voltage angle θ. Consequently, buses can be sorted into three categories when two of the above quantities are given for each bus [9]

- *Voltage-controlled* (*PV*) *bus*: Active power and voltage magnitude are known. Additionally, reactive power limits are provided depending on the characteristic of specific devices. Examples of this type of buses are the ones with generators, synchronous condensers, and static var compensators.
- *Load (PQ) bus*: Active and reactive power are assigned. Normally this type of bus is connected to loads, which are assumed to have constant power consumption.
- *Slack (swing) bus*: Voltage magnitude and phase angle are given. Since the power losses in the system are not measurable, at least one bus must have unfixed P and Q, the slack bus is the bus with known voltage (both magnitude and angle).

To obtain the network equations of a balanced power system, each component of the system is modelled in terms of one phase equivalent circuit. The relationships between network bus voltages and currents can be illustrated by node equations in terms of the node admittance matrix [9]

$$\begin{bmatrix} \widetilde{I_1} \\ \widetilde{I_2} \\ \dots \\ \widetilde{I_n} \end{bmatrix} = \begin{bmatrix} Y_{11} & Y_{12} & \dots & Y_{1n} \\ Y_{21} & Y_{22} & \dots & Y_{2n} \\ \dots & \dots & \dots & \dots \\ Y_{n1} & Y_{n2} & \dots & Y_{nn} \end{bmatrix} \begin{bmatrix} \widetilde{V_1} \\ \widetilde{V_2} \\ \dots \\ \widetilde{V_n} \end{bmatrix} \qquad (2\text{-}13)$$

where

n is the total number of buses in the system

Y_{ii} is the self-admittance of node i

= sum of all the admittances terminating at node i

Y_{ij} is mutual admittance between nodes i and j

= negative of the sum of all admittances between nodes i and j

$\widetilde{V_i}$ is the phasor voltage to ground at node i

$\widetilde{I_i}$ is the phasor current flowing into the network at node i

In this network equation, the effects of the generators, nonlinear loads and other components (synchronous condenser, dynamic reactive compensators) connected to the system buses are indicated in the currents. Constant impedance (linear) loads are put in as part of the node admittance matrix [9].

If the current matrix in Equation 2-13 is known for all buses, then it can be solved as a linear equation. However, in real case, the current injections are not known for most of the nodes. The current at any node k is a function of P, Q and $\tilde{V}$

$$\widetilde{I_k} = \frac{P_k - jQ_k}{\widetilde{V_k}^*} \qquad (2\text{-}14)$$

In regard to the different bus types, for the PV buses, only P and the magnitude of $\tilde{V}$ are known; and for the PQ buses, only P and Q are explicitly stated. With the different limit conditions of different types of buses, Equation 2-13 becomes a nonlinear power-flow equation. Therefore, iteration techniques such as Gauss-Seidel or Newton-Raphson method are implemented to solve the resulting nonlinear system of equations [9]. The principle of Newton-Raphson method is illustrated in the next section.

2.3 Newton-Raphson Solution Method

Newton-Raphson method is a commonly used iterative approach to solve nonlinear equations. Compared to Gauss-Seidel method, it has a very fast convergence rate and the computation time increases linearly with system size. And this method is particularly suited for applications involving large computations requiring very accurate solutions [9].

Newton-Raphson approach starts with an initial estimate of all unknowns in the power system, including phase voltage at PQ buses and voltage angles at PV buses. Next, Taylor expansion is written for each of the power balance equations in network Equation 2-13. It should be noted that if the quantity corrections are close to the true solution, the terms of higher order in the expanded Tylor equation can be ignored. Then, this results a linear set of power equations that can be solved [9].

To apply Newton-Raphson method, polar forms of the vector quantity is needed. For the k^{th} bus power equation

$$\widetilde{S_k} = P_k + jQ_k = \widetilde{V_k}\widetilde{I_k}^* \quad (2\text{-}15)$$

Knowing from Equation 2-13 that

$$\widetilde{I_k} = \sum_{m=1}^{n} Y_{km}\widetilde{V_m} \quad (2\text{-}16)$$

Substituting the current $\widetilde{I_k}$ to Equation 2-15

$$P_k + jQ_k = \widetilde{V_k}\sum_{m=1}^{n}(G_{km} - B_{km})\widetilde{V_m}^* \quad (2\text{-}17)$$

The product of voltage $\widetilde{V_k}$ and $\widetilde{V_m}^*$ can be expanded as

$$\widetilde{V_k}\widetilde{V_m}^* = (V_k e^{j\theta_k})\left(V_m e^{-j\theta_m}\right) = V_k V_m e^{j(\theta_k - \theta_m)} \quad (2\text{-}18)$$

$$= V_k V_m(cos\theta_{km} + jsin\theta_{km})$$

Therefore, P_k and Q_k are derived separately by combining Equation 2-17 and 2-18

$$P_k = \widetilde{V_k} \sum_{m=1}^{n} (G_{km} V_m cos\theta_{km} + B_{km} V_m sin\theta_{km}) \quad (2\text{-}19)$$

$$Q_k = \widetilde{V_k} \sum_{m=1}^{n} (G_{km} V_m sin\theta_{km} - B_{km} V_m cos\theta_{km}) \quad (2\text{-}20)$$

Now, P and Q at each bus can be computed using a function of voltage magnitude V and angle θ of all buses.

Following the Newton-Raphson method, the linear system of equation can be described as:

$$\begin{bmatrix} \Delta P \\ \Delta Q \end{bmatrix} = \begin{bmatrix} \frac{\partial P_1}{\partial \theta_1} & \cdots & \frac{\partial P_1}{\partial \theta_n} & \frac{\partial P_1}{\partial V_1} & \cdots & \frac{\partial P_1}{\partial V_n} \\ \cdots & \cdots & \cdots & \cdots & \cdots & \cdots \\ \frac{\partial P_n}{\partial \theta_1} & \cdots & \frac{\partial P_n}{\partial \theta_n} & \frac{\partial P_n}{\partial V_1} & \cdots & \frac{\partial P_n}{\partial V_n} \\ \frac{\partial Q_1}{\partial \theta_1} & \cdots & \frac{\partial Q_1}{\partial \theta_n} & \frac{\partial Q_1}{\partial V_1} & \cdots & \frac{\partial Q_1}{\partial V_n} \\ \cdots & \cdots & \cdots & \cdots & \cdots & \cdots \\ \frac{\partial Q_n}{\partial \theta_1} & \cdots & \frac{\partial Q_n}{\partial \theta_n} & \frac{\partial Q_n}{\partial V_1} & \cdots & \frac{\partial Q_n}{\partial V_n} \end{bmatrix} \begin{bmatrix} \Delta\theta_1 \\ \cdots \\ \Delta\theta_n \\ \Delta V_1 \\ \cdots \\ \Delta V_n \end{bmatrix} \quad (2\text{-}21)$$

or

$$\begin{bmatrix} \Delta \boldsymbol{P} \\ \Delta \boldsymbol{Q} \end{bmatrix} = \begin{bmatrix} \frac{\partial \boldsymbol{P}}{\partial \boldsymbol{\theta}} & \frac{\partial \boldsymbol{P}}{\partial \boldsymbol{V}} \\ \frac{\partial \boldsymbol{Q}}{\partial \boldsymbol{\theta}} & \frac{\partial \boldsymbol{Q}}{\partial \boldsymbol{V}} \end{bmatrix} \begin{bmatrix} \Delta \boldsymbol{\theta} \\ \Delta \boldsymbol{V} \end{bmatrix} = J \begin{bmatrix} \Delta \boldsymbol{\theta} \\ \Delta \boldsymbol{V} \end{bmatrix} \quad (2\text{-}22)$$

where the matrix of partial derivatives is defined as a *Jacobian.* The correction ΔP and ΔQ are calculated from:

$$\Delta P_k = -P_k + \widetilde{V_k} \sum_{m=1}^{n} (G_{km} V_m cos\theta_{km} + B_{km} V_m sin\theta_{km}) \quad (2\text{-}23)$$

$$\Delta Q_k = -Q_k + \widetilde{V_k} \sum_{m=1}^{n} (G_{km} V_m sin\theta_{km} - B_{km} V_m cos\theta_{km}) \quad (2\text{-}24)$$

Since Equation 2-13 becomes a linear set of equations in matrix form, assuming the active power P and reactive power Q at each bus are known for all buses, the iteration algorithm to solve this problem is followed as:

a) The iterations start with an initial estimate of all absent voltage magnitudes $V_1^0, V_2^0, \dots, V_n^0$, and angles $\theta_1^0, \theta_2^0, \dots, \theta_n^0$. Usually, the "flat start" is the used, which set all voltage angles to zero and all voltage magnitudes to 1.0 p.u.

b) Based on the most updated voltage angle and magnitudes numbers, solve the power balance Equation 2-23 and 2-24 to get the correction value $\Delta P_1^0, \Delta P_2^0, \dots, \Delta P_n^0$ and$\Delta Q_1^0, \Delta Q_2^0, \dots, \Delta Q_n^0$.

c) Use the linear Equation 2-21 to get the differences of the voltage magnitudes and angles $\Delta V_1, \Delta V_2, \dots, \Delta V_n$, and $\Delta\theta_1, \Delta\theta_2, \dots, \Delta\theta_n$.

d) The next estimated values of voltage magnitudes $V_1^1, V_2^1, \dots, V_n^1$ and angles $\theta_1^1, \theta_2^1, \dots, \theta_n^1$ are updated based on:

$$\theta_i^1 = \theta_i^0 + \Delta\theta_i$$

$$V_i^1 = V_i^0 + \Delta V_i$$

e) Check the stopping conditions: Assume the updated V_i and θ_i are close enough to the real value when the correction of ΔP and ΔQ are below the specified tolerance and the repeated process will be terminated; otherwise back to step 2.

Note that during the iteration process, the Jacobian has to be recalculated at each step.

Knowing that in real system, only reactive power P and the magnitude of V are specified for the PV buses while PQ buses have fixed real power P and reactive power Q. Hence, the corresponding ΔQ and $\Delta\theta$ are unknown for specific PV bus. Nevertheless N-R iteration method can still solve for the power balance equation on a PV bus [9].

2.4 MATPOWER Toolbox

MATPOWER is a package of MATLAB M-files for solving power flow and optimal power flow problems. MATPOWER was developed by Ray D. Zimmerman, Carlos E. Murillo Sanchez and Deqiang Gan of PSERC at Cornell University under the direction of Robert J. Thomas. In this research, the MATPOWER is used to run the Newton-Raphson power flow program. To start the N-R power flow simulation, three simple steps are briefly introduced in this section [10]

1. Prepare the input data specifying all of the test power system parameters;
2. Call for the power flow routine to run the simulation;
3. Access and save the power flow results.

Firstly, in MATPOWER toolbox, the input data files of test power system are already saved in a set of documents packaged in the folder "MATPOWER case". Using the command **loadcase** can access the input data documentation. Traditionally, the case can be defined by the variable **mpc**, which stands for MatPower Case. By default, the input of the case data consists of bus data, generator data, branch data as well as generation cost information [10]. The format of the data document is available in Appendix B.

```
>> mpc = loadcase (casefilename);
```

After loading the case file, a simple Newton power flow simulation with default options can start to work by calling **runpf** with the specific case file name [10].

```
>> results = runpf (casedata);
```

Alternatively, if a parameter modification of system input is needed before requesting the power flow simulation, for example, to rewrite the real power demand on bus 2 to 30 MW in the 30-Bus test system, command script can be wrote as follows [10]:

```
>> define_constants;
>> mpc = loadcase('case30');
>> mpc.bus (2, PD) = 30;
>> runpf (mpc);
```

The **define_constants** is the command statement that denotes the data in matrix to serve as defined column value. For example, it names the "real power demand" column of the **bus** matrix by the name **PD** without counting that it is the 3rd column in the matrix. The detail information of the column name is available in Appendix B.

When the iterative computations converge, MATLAB prints out the results on the screen automatically, including a set of the input MATPOWER case, and some additional data in some of the existing data fields. Specifically, the bus data shows the voltage, angle and total generation and load demand at each bus. The branch data gives the power flows and power losses in each line. The generator data involves the generators real power and reactive power output. All these variables of the outputs can be documented by providing a file name in order to easily access later in the program. For example, after running the AC power flow on the 30-bus system in case30.m, to obtain the solution of the power flow function, the real power generation of generator 6 and the power flow on branch 12 [10].

```
>> define_constants;
>> mpc = loadcase ('case')
>> results = runpf (mpc);
>> gen6_output = results.gen (6, PG);
>> branch12_flow = results.branch (12, PF);
```

All the outcomes of the power flow function are stored in a results file and can be defined to serve as specific column name as shown in Table 2-2.

Table 2-2. Power Flow Results *[10]*

name	description
`results.success`	success flag, 1 = succeeded, 0 = failed
`results.et`	computation time required for solution
`results.order`	see `ext2int` help for details on this field
`results.bus(:, VM)`†	bus voltage magnitudes
`results.bus(:, VA)`	bus voltage angles
`results.gen(:, PG)`	generator real power injections
`results.gen(:, QG)`†	generator reactive power injections
`results.branch(:, PF)`	real power injected into "from" end of branch
`results.branch(:, PT)`	real power injected into "to" end of branch
`results.branch(:, QF)`†	reactive power injected into "from" end of branch
`results.branch(:, QT)`†	reactive power injected into "to" end of branch

† AC power flow only.

Chapter 3
Contingency Analysis

When integrating a utility-scale PV generation system into the existing power system, a primary concern is the potential security problems of the system performance. For the evaluation of the security performance of a power system is essential to examine the ability of the system to withstand the loss of any single component. Considering the power transfer capacity and stability limits of the system, failure of a single component in the system could have severe consequences for system operation [11].

Regarding to the stability requirements in electric power system, voltage and power flow are two significant factors in monitoring system performance [9]:

a) ***Bus voltages***. Voltage magnitude of all buses in the system should stay in an acceptable range. Both the utility equipment and customer equipment are designed to work at a certain voltage rating for effective operation. Extended operation of the equipment at voltages away from its proper limits could severely influence their functioning and possibly result in failure.

b) ***Line flows***. Power flow through an AC transmission line must be limited in a security range. Power transmission capability of a power line is determined by manufacturer's standard that consider voltage regulation, thermal limits and system stability. These are the general limiting factors that set the maximum allowable power transmitted on line.

In the transmission system, both the voltage at each terminal and power flows are significantly influenced by the network configuration, system generation and load distribution. Therefore, any disturbances or changes of the system could impose system operation limits violation and consequently system outage.

In this chapter, N-1 contingency analysis is discussed to evaluate and test system security performance. The protective and repairing practices should be implemented accordingly to guarantee the system stable operation. The mitigation practices such as reactive power

compensation and line reconstruction will be covered in this chapter. By identifying unacceptable voltage magnitude and power flow, this analysis allows the utility company to predict contingency scenarios that may arise in the future operation [12]. Newton-Raphson power flow function in MATPOWER toolbox is applied in this part for contingency identification.

3.1 Voltage Control

According to the IEEE standard, the voltage stability is defined as the capability of an electric power system to keep satisfactory voltage levels in all nodes under normal operations or after given a system disturbance [9]. This concept presents the idea of the robustness of a power system which is measured by its ability to preserve the balance between the demanded load and the generated power. The system can be in an unstable status especially for the voltages when there is a disturbance, increment of load and topology changes in the network, that induce a severe and uncontrollable voltage decrement [9].

Voltage collapse is a typical phenomenon that might be present in a highly loaded area in an electric power system. It is a reaction of the system when sequential events occur together with voltage instability, leading to a low unacceptable voltage level in a significant area of the power system. After these disturbances, the voltages usually cannot automatically be restored to original normal point by itself and consequently may lead to a major blackout [9]. Generally, there are different factors contributing to the voltage collapse:

- Increase of load demand
- Reaching of the reactive power limitation of generating units, synchronous condensers
- The operation of TAP-changing in transformers
- The loss of transmission lines, transformers and generators

It should be noted that most of these changes may have significant effects in the generation, consumption and distribution of reactive power and eventually lead to voltage instability. Therefore, the primary remedy principle of voltage instability is improving the system's reactive power capacity. This is generally referred to reactive power compensation, and it is completed via devices attached to the line or bus liker [9]:

(a) Sources or sinks of reactive power, such as shunt capacitors, shunt reactors, synchronous condensers, and static var compensators (SVC).
(b) Line reactance compensators, such as series capacitors.
(c) Regulated transformers, such as tap-changing transformers and boosters.

According to the description of Prabha Kunder [9], synchronous condensers and SVCs provide active compensation; the reactive power supported or consumed by them is automatically accommodated according to the bus voltage level to which they are connected, while shunt capacitors and reactors, and series capacitors provide passive compensation. They are either permanently connected to the transmission and distribution system, or switched and the network characteristic is modified when these devices are controlling the voltage [9].

Based on these potential severe voltage problems, it is necessary to have voltage stability analysis of the power system. Some of the system models used for the analysis of voltage stability are based on dynamic analysis and others on static analysis [9]:

a. *Dynamic Analysis.* These approaches involve some numerical computations of the overall differential and algebraic network equations derived from the power system model and resemble transient analysis. As complicated differential computation process is required, these methods usually consume large amounts of time.
b. *Static Analysis.* They are focused on a particular steady state of the system operation. A set of network power balance equations is simplified to merely algebraic equations. Conventionally, static analysis of voltage stability depends on power flow programs. Stability characteristic is determined by generating V-P and Q-V curve at selected load buses by computing the series of power flows. These curves are generated for individual buses and therefore the stability information are established by emphasizing each bus independently.

In this research, static analysis accompanying with Q-V curve simulation is applied for the test system. The Q-V curve depicts the relationship between voltage and the reactive power and especially gives out the sensitivity information and variation of bus voltages with changing reactive power. Therefore, it can provide useful information to gain insight into causes of voltage stability problems and determining reactive power compensation in the system.

Q-V curves at selected buses can be generated by solving series AC power flow program after initial operating condition is given for the test power system. The AC power flow can be computed in MATPOWER by using the Newton-Raphson power flow program. With various reactive power injection on selected bus, power flow program may have different convergences. The general procedure for finding the amount of reactive power required to bring the voltage back to an acceptable operation point is to obtain the sensitivity characteristic of the target location.

Figure 3-1 illustrates the Q-V curve simulated at bus 3 in IEEE 24-bus Reliability Test System. It is produced by successive power-flows with variable reactive power load Q at Bus 3. This plot illustrates that the voltage V will start to drop when incrementally changing the load Q. This is because of the limitation of generator reactive power capacity in this system. When the reactive power demand exceeds the available reactive power capacity in the system, voltage collapse happens and could lead to instability of the system. Eventually, the power flow does not converge and there is no operating point existing anymore.

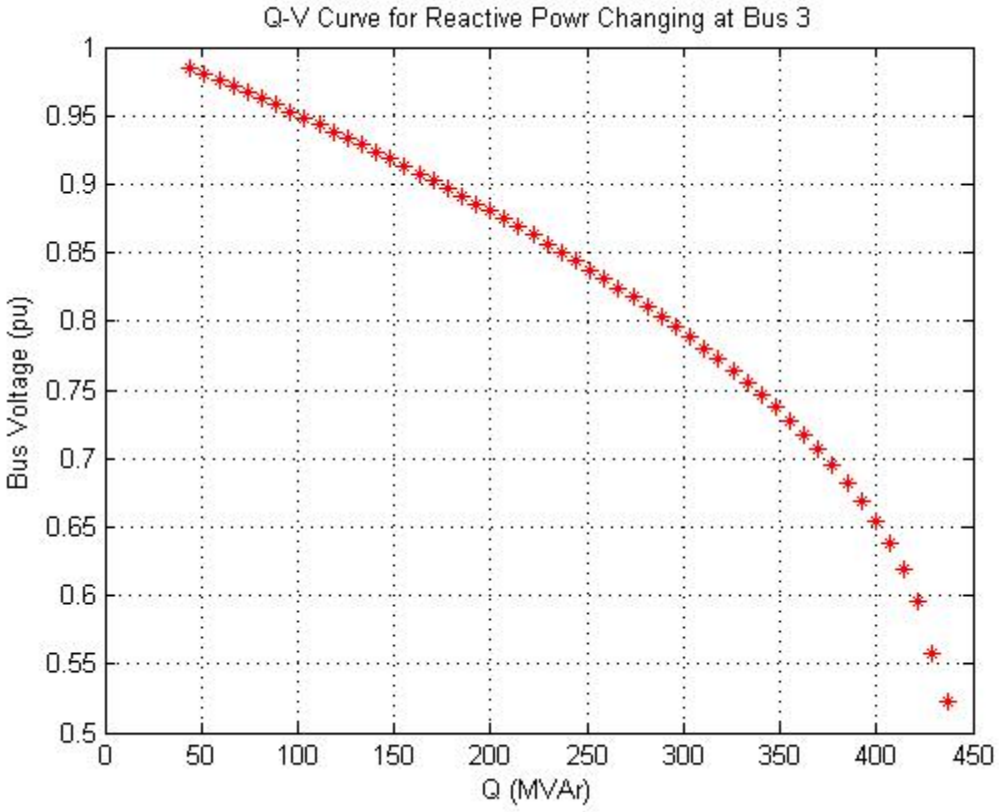

Figure 7. Q-V curve (Bus 3 in IEEE 24)

In this work, the methodology of computing the amount of reactive power compensation using Q-V characteristic curve is implemented using the following steps：

1. Select the load bus at which has potential voltage stability problem. This load bus should be examined and identified to have the probability to be influenced by voltage collapse.
2. Solve the initial operating status by AC power flow function in MATPOWER and get the voltage profile $V_0$and reactive power demand Q_0on this bus, where the voltage collapse is supposed to be existence on this bus.
3. The reactive power injection should be allowed to adjust in the process of the Q-V analysis.
4. Increase the reactive power injection Q_0 on this selected bus by 0.2 * Q_0 and keep the rest of the system data the same. Run the power flow function and obtain the new voltage value $V_1$with respect to the increased reactive power.
5. Decrease the reactive power injection Q_0 on this selected bus by 0.2 * Q_0 and keep the rest of the system data the same. Then run the power flow function with the decreased reactive power injection to get the corresponding bus voltageV_2.
6. Compare the V_1 and V_2 with 1.0 p.u. and determine the one that is closer to the 1.0 p.u voltage and record the corresponding reactive power Q'
7. Calculate the sensitivity of $\frac{dQ}{dV}$ by

$$\frac{dQ}{dV} = \frac{Q' - Q_0}{V_1 - V_2} \qquad (3\text{-}1)$$

8. The compensation reactive power Q_{com} required to increase the voltage to stable operating point (assume $V_{goal} = 0.98\, p.u.$) is determined by

$$Q_{com} = \frac{dQ}{dV} * (V_{goal} - V_0) \qquad (3\text{-}2)$$

Therefore, with the Q-V characteristic curve, the demanded capacity of the reactive power compensation to step up the voltage is estimated. Accordingly, this can be used to select appropriate compensation devices.

3.2 Power Line Mitigation

Branch power flow off-limits is another important issue of system instability. The power flow capability on each line depends on the thermal effects of the line current. This is because the heat produced by current flow in transmission lines has two undesirable effects [9]:

- Annealing and gradual loss of mechanical strength of the aluminum conductor caused by prolonged working under extreme temperature
- Growing sag and decrease clearance to ground due to heat in the line environment

In order to prevent off-line-limits operation, maximum permissible power flowed through transmission line is usually set to a value well below its full capacity. Regarding to different operation circumstances, the power rating of lines may be set to different levels accordingly. Normally, there are 3 classes of power rating (MVA) for each individual line, including the long term rating, short term rating and emergency rating. Generally, long term rating, the allowable operating power flow capacity of the line in the long term, has the smallest value while the emergency rating has the maximum value that can only be used for a short time during contingency circumstances. At some time, the three ratings are set to be same.

To address the off-line-limits operation, the algorithm needs to find out the power flow of each line and check the operation status. However, unlike the voltage magnitude, the line flow of each line is not directly available after each AC power flow iteration. Therefore, computation of line flow is necessary before identifying violation. The practical model of the π equivalent transmission line model is presented in Chapter 2. Given the voltage and power injections of the bus, Equation 2.12 can be directly utilized to verify the power flow through the transmission line.

In this research, if the designed rating of the line exceeds the emergency rating value, the system is regarded as branch violation and a new power line is suggested to be constructed to ensure continuous power supply.

3.3 N-1 Contingency Analysis using AC Power Flow

Electrical utilities are often required to maintain N-1 redundancy for all transmission lines, generating units, and the primary distribution components to guarantee that the entire system can be restored and continues operating if any single component fails (N-1 components still available) [13]. N-1 contingency analysis is a fast automated process for assessing power system performance following loss of one single element. This approach incorporates different conditions of contingencies in order to identify potential risks such as voltage collapse or power line overloads. In this research, the N-1 contingency analysis with single line outage is examined.

To start the N-1 contingency analysis, a contingency situation is arranged assuming that a transmission line is detected with fault and removed from service. With the loss of a single transmission line, the network configuration changes and the power that flowed through the entire system is redistributed among the remaining network. This single line failure will result in system impedance increment, hence the power flow on remaining lines steps up. This increment in power transmitted together with the growth of system impedance leads to higher voltage drops along the transmission lines [11]. Consequently, this could result in voltage collapse and branch power flow off-limits.

A general block diagram outlining the proposed algorithm using AC power flow in MATLAB is shown in Figure 3-2.

Assume the algorithm input is the database of the testing system containing the detail information of buses, branches and generators. With the case data of the test system, the first step of the procedure is to pick up a branch to fail by set the service status to zero in MATLAB, while keeping the rest of the system data the same. Then the AC power flow computation is accomplished with the line outage. After the power flow simulation, the bus voltage profile and power flow of each line are checked to ensure that:

1. The power flow on each transmission line is lower than the designed emergency rating value
2. The voltage magnitude of all buses are staying in the acceptable range [0.95pu, 1.05pu]

If any violation of these two parameters happens, the violating data will be recorded. The checking process will repeat for each line in the system.

All the above steps are iterated for every line outage circumstance. After all line outage cases are completed, the violation results will be displayed on screen.

With the contingency simulation results, the demand for voltage control and power line mitigation can be predicted and some recommendations and measures for risk prevention and reduction can be proposed as discussed in the previous section.

In this research, this process can bring practical advantages for the risk identification and mitigation cost estimation of a PV-penetration system to achieve a secure system.

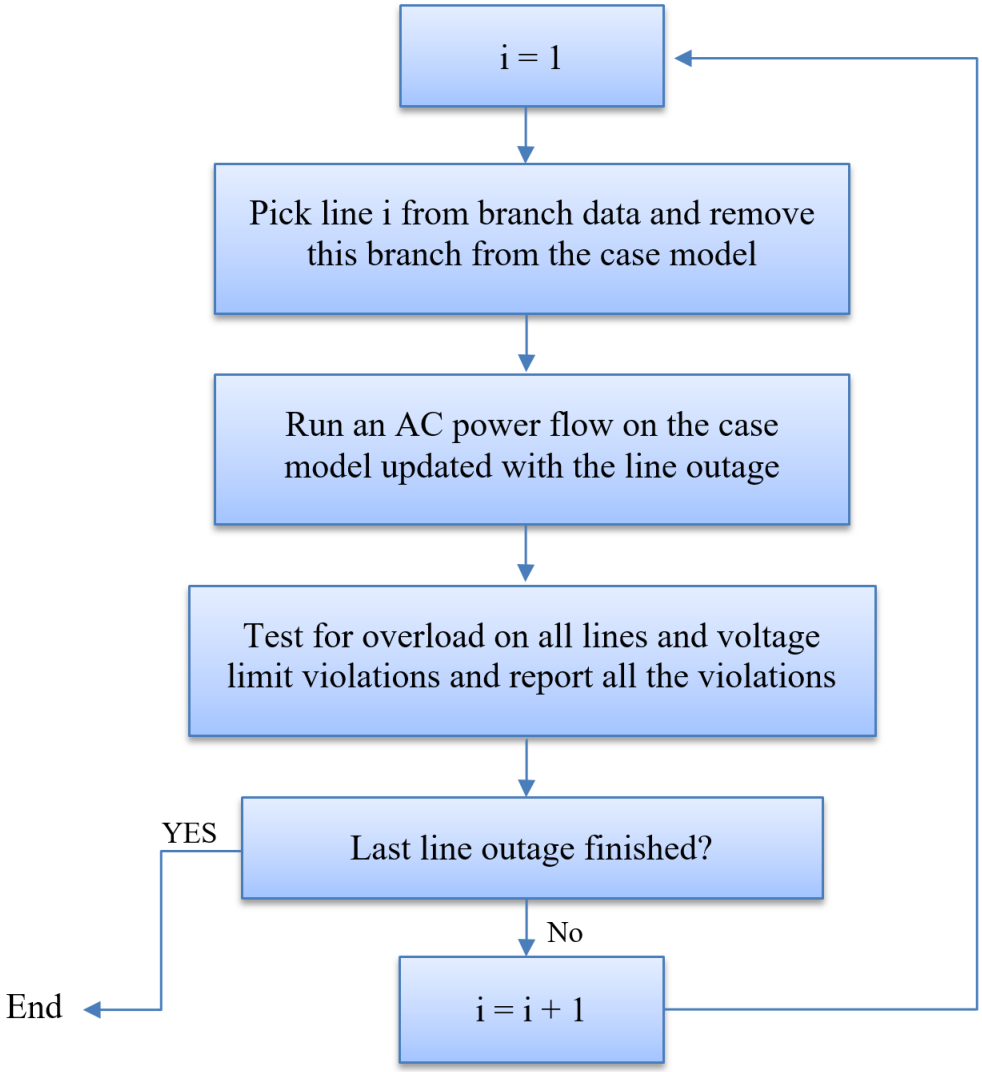

Figure 8. AC power flow N-1 contingency analysis algorithm

Chapter 4
Reliability Evaluation using Monte Carlo Simulation

Power systems have developed over decades with the goal of providing a reliable supply of electrical energy to customers. However, conventional generating units present reliability problems due to the system random nature, such as randomly occurring failures, forced outages of plants, the absent of facilities for regular scheduled maintenances, while a solar energy generating unit has to face the problem of the chronological random nature of the solar radiation level and the dependencies associated with the power output of every PV generating unit at the site location [14]. Therefore, reliability performance of the system depends on both the PV generation performance and the conventional unit operation.

In our research, the solar power output is modeled with the major variable of the random time-correlated chronological solar radiation conditions. To assess the reliability performance of conventional generation facilities, utilities usually keep a record of the operation events as they occur. Some particular system performance data usually involved are [15]:

- System availability;
- Number of hours of interruption;
- Number of incidents;
- Estimated unsupplied energy.

With the fully knowledge of the system's characteristic parameters, appropriate system model can be developed to reflect the system operation [15]. Once a system model is derived, the reliability performance can be simulated on the basis of the load characteristic and expected generation performance. Generating unit's operation cycle can be predicted by applying probability density distribution with Monte Carlo Simulation. As for the solar energy output, it can be calculated according to the site solar irradiation data. The load characteristics are normally processed from past experience and requirements. Then the conventional generating capacity adequacy of a system can be easily evaluated.

In this chapter, the Monte Carlo Simulation is introduced to obtain operation cycle of each conventional generating unit in a long period. The development of system generation and load model are included. Also a method of estimating solar system output is presented. The combination of these models are used to assess the system reliability performance. The adequacy index – Loss of Load Probability is calculated for the system.

4.1 Monte Carlo Simulation

It should be noted that in the performance of n identical power systems all will exhibit different behavior, including the number of failures, the residence time between failures and the restoration times. The simulation process is intended to achieve the real characteristic performance in simulated time and produce the expected value of the reliability parameters [15].

Considering the example of tossing a coin, the probability of getting a head or tail in a single throw is known to be $\frac{1}{2}$. However, with the understanding of the frequency definition, this can usually be approximated by [15]

$$\text{P (of the head occurring)} = \lim_{N\to\infty}\left(\frac{H}{N}\right) \qquad (4\text{-}1)$$

where

H is the number of heads

N is the number of tosses

After tossing a single coin 20 times, the results obtained are shown pictorially in Figure 4-1. The plot illustrates that [15]:

(a) A small number of experiments (simulations) gives out a very poor estimation of the probability.

(b) The value of probability fluctuates but has a tendency toward the true value when additional experiments are performed.

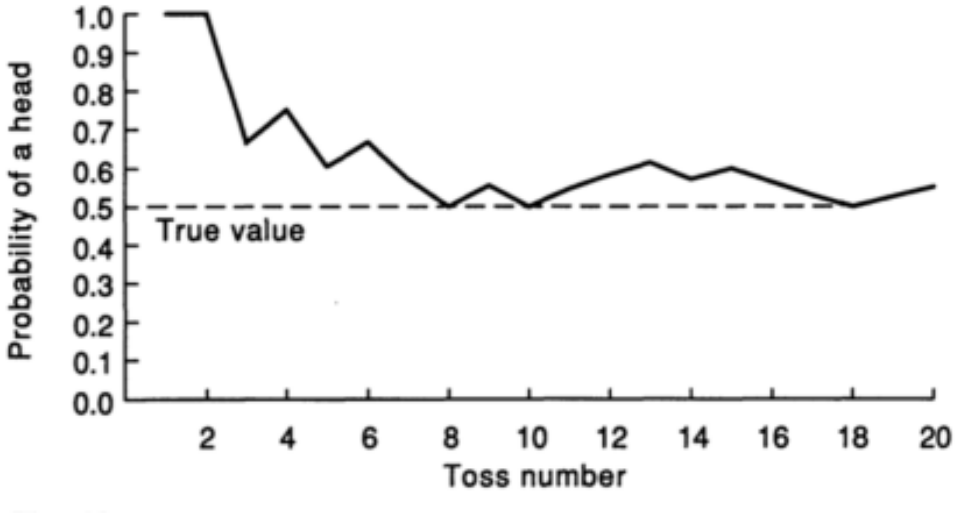

Figure 9. Probability of tossing a head *[15]*

When utilizing a system model to simulate system generation availability and unavailability, the random occurrences of failures of the components due to their stochastic behavior are important factors for power engineers to consider.

A widely used simulation approach for power system reliability evaluation is the Monte Carlo Simulation (MCS). To apply this method, the prediction of system operating states are determined by random numbers and these values can be manipulated to simulate the characteristic of a probability density function (PDF). Generally, the random variables U is initially uniformly generated in the range of zero to one by a random variable generator. Then they are transformed to numbers indicating a non-uniform probability distribution.

An example of Monte Carlo application of power system simulation is demonstrated below. For power system reliability analysis, the exponential distribution is assumed to be suited for generator state residence time. As plotted in Figure 4-2, the state probability density function for a component in power system is exponentially distributed with a parameter λ as:

$$f(x,\lambda) = \begin{cases} \lambda e^{-\lambda x} & x \geq 0 \\ 0 & x < 0 \end{cases} \qquad (4\text{-}2)$$

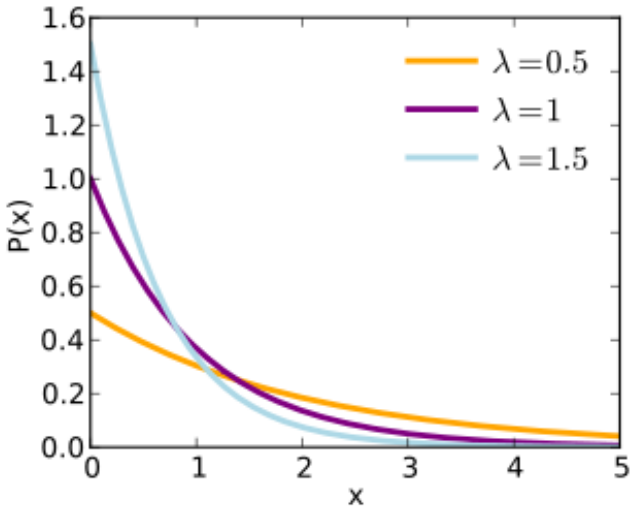

Figure 10. Exponential distribution function *[16]*

The cumulative density function (CDF) of the exponential probability density function is defined as the probability that variable will be less than t. The CDF $F(t)$ can be obtained by [17]:

$$F_T(t) = P(x \leq t) = \int_0^t f(x)dx = 1 - e^{-\lambda t} \qquad (4\text{-}3)$$

the plot of CDF is uniformly distributed in the interval [0,1] as shown in Figure 4-3.

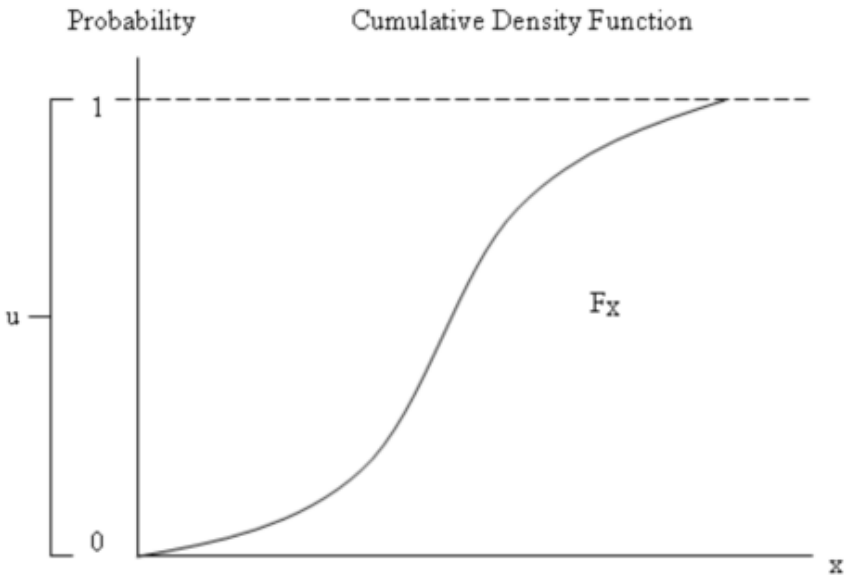

Figure 11. Cumulative density function *[18]*

Then it can be converted to obtain the exponential variable t by applying [18]:

$$F(t) = 1 - e^{-\lambda t} = U \quad (4\text{-}4)$$

$$e^{-\lambda t} = 1 - U \quad (4\text{-}5)$$

Since $(1 - U)$ is uniformly distributed in the same way as U in the range between zero and one [19],

$$e^{-\lambda t} = U \quad (4\text{-}6)$$

$$-\lambda t = ln(U) \quad (4\text{-}7)$$

So that

$$t = -\frac{1}{\lambda} ln\, U \quad (4\text{-}8)$$

where

U is a uniformly distributed random number sequence between [0,1].

This process of generating exponentially distributed random variates t is the Monte Carlo Simulation Method. This the essential method which used to generate the operation cycle of conventional generating units in the following sections.

4.2 Modeling of System Generation

To apply the Monte Carlo Simulation techniques to power system reliability evaluation, the first priority is to select an appropriate system model representing the generating system. In this research, the conventional generation system model is used as shown in Figure 4-4. It simplifies the generation and load models.

By applying this model, the total system generation can be examined to determine its adequacy level to meet the system load demand. It should be mentioned that the reliability parameter derived from this model does not specify any generation deficiencies at any particular customer load location but represents the overall adequacy degree of the generation system [15].

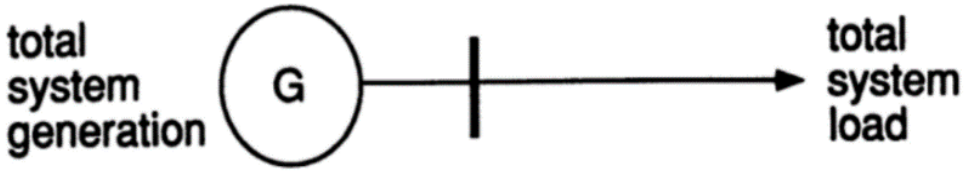

Figure 12. System model *[19]*

Normally, each generating units is assumed to be independent of each other and act as base load units. In this case, the two-state model can suit each single unit of the system as shown in Figure 4-5. Assume each unit are repairable and the time of repairing and operating are exponentially distributed. The unit can reside in one of two states at a time. The up-state and down-state of the unit stand for generation availability and unavailability correspondingly. λ and μ are state transition parameters [19].

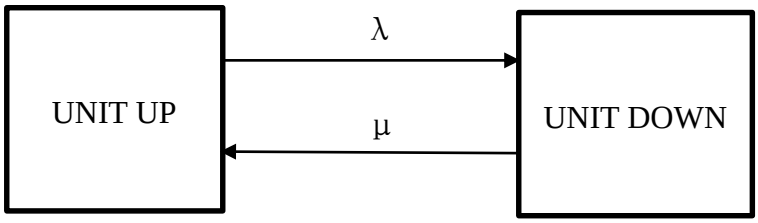

Figure 13. Two-state model for a base load unit in terms of transition diagram *[19]*

According to the historically utilities recording of the unit failures and the duration of failures, a typical states diagram of generator can be pictorially illustrated as Figure 4-6. In this figure, TTF is the time to failure and TTR the time to repair and they are specified for each event.

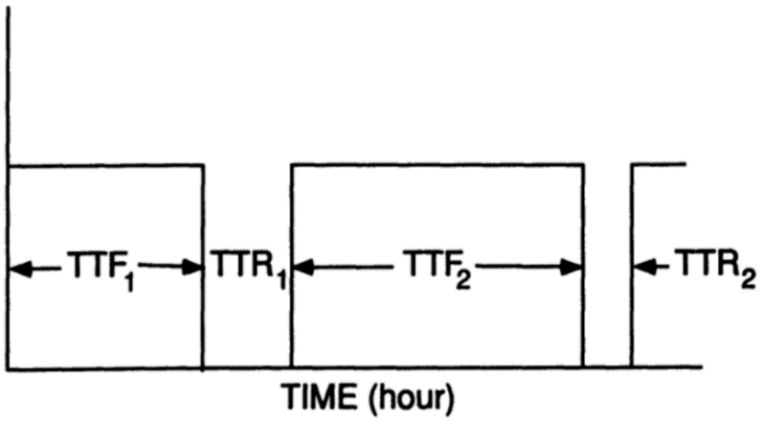

Figure 14. Typical states duration of a two-state model *[19]*

Additionally, two essential parameters can be achieved on the basis of the recording operation data TTF and TTR [15]:

(a) MTTF: the mean (average) time to failure

(b) MTTR: the mean (average) time of the facility for restoration

It is noteworthy that these two parameters referred to generator reliability data play an important role in predicting system generation adequacy.

Given the MTTF and MTTR of a two-state model, generating facility operation states by MCS can be achieved as follows. Assuming all the generating facilities in the system are repairable and the time of operating and repairing are exponentially distributed. Estimation of the variable TTF and the TTR can be obtained by drawing exponential distributed random values $U_1, U_2$with parameters $\lambda = 1/MTTF$ and $\mu = 1/MTTR$ respectively [19],

$$TTF = -\frac{1}{\lambda} ln\, U_1 = -MTTF\, ln\, U_1 \qquad (4\text{-}9)$$

$$TTR = -\frac{1}{\mu} ln\, U_2 = -MTTR\, ln\, U_2 \qquad (4\text{-}10)$$

With the values of TTF and TTR, an artificial sequence of each unit operating cycles (up-down) can be generated for a sampling time and then the total system capacity available can be obtained by adding the state duration cycles of all units together as shown in Figure 4-7 [19].

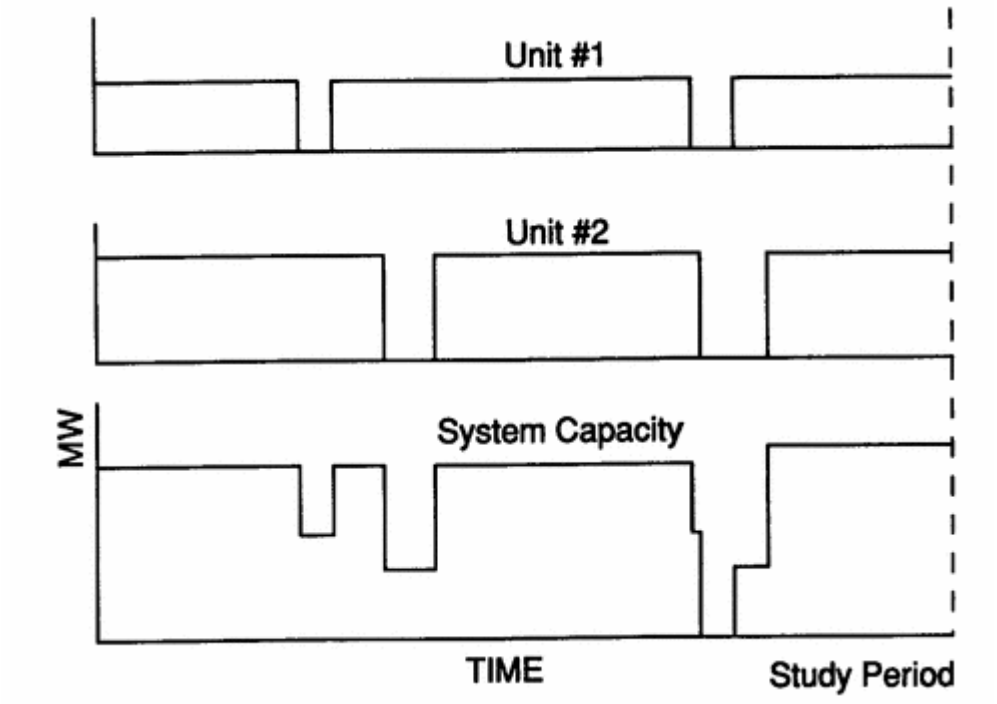

Figure 15. Available capacity models of each unit and the system *[19]*

4.3 Solar Power Output

When designing the solar PV system, the output power from a PV generating unit is mainly determined by the amount of solar radiation at the particular site. Detailed irradiation data for this study can be accessed from the National Renewable Energy Lab website and the data link is available in Appendix A [20]. Besides the atmospheric conditions, the PV system power output also depends on characteristics of the system equipment. As mentioned in the Chapter 1, a typical utility-scale PV system is composed of PV module/array, power conditioner, DC/AC inverter and

the grid load. In general, PV array convert solar irradiation to DC current. The DC current flows through a power conditioner and finally delivered to the grid in AC current. The hourly energy output of a PV system is given by [21]

$$E_{pv} = A_{pv} \times E_{sun} \times \eta_{pv} \times \eta_{inv} \times \eta_{wir} \quad (4\text{-}11)$$

where

A_{pv} is the land area covered by the PV panels in m^2;

E_{sun} is the hourly solar irradiation in W/m^2 ;

η_{pv} is the efficiency of PV module;

η_{inv} is the efficiency of inverter;

η_{wir} is the efficiency of wires.

4.4 Modeling an Annual Load Curve

A chronological electricity load model can be defined for the reliability assessment of the system. One of the main characteristic of the chronological load is that the load changes with the weather, time of the day, the day of the week and the week of the year. To develop time varying customer load model, the hourly load characteristics has to be combined with the annual/weekly/daily peak load data to generate annual models. Three type of load characteristic data can enumerate the load levels including [22]:

a) 24-hour daily load as a percentage of the daily peak load;
b) 7-day weekly load as a percentage of the weekly load;
c) 52-week yearly load as a percentage of the yearly peak load;

With profile of the annual peak load data and the above daily/weekly/yearly load percentage, the hourly load $L(t)$ for hour t can be calculated using the following formula [22]:

$$L(t) = L_y \times P_w \times P_d \times P_h(t) \quad (4\text{-}12)$$

where

L_y is the annual peak load in Watt

P_w is the percentage of weekly load in terms of the annual peak

P_d is the percentage of daily load in terms of the weekly peak

$P_h(t)$ is the percentage of hourly load in terms of daily peak.

It is noteworthy that the hourly load demand $L(t)$ only represents the hourly peak load of the system , giving $52 \times 7 \times 24 = 8736$ independent values for a year.

The hourly peak electricity demand profile in the IEEE 24 bus Reliability Test System (IEEE-RTS) can be developed using the approach described above. The annual peak load is 2850 MW. The daily/weekly/yearly load percentage data are available in Appendix C.

Figure 4-9 shows the load duration curves of the electricity demand over a period of 24 hours in 12 months. The demand varies significantly over the 24 hours in a day. Typically, demand begins to increase around 5 am as some of the industry starts to running and people prepare to work. By 8 am, the electricity power demand continues to go constantly up until shortly before noon, when it starts to drop down a little bit due to the lunch period. The morning trend of the curve is again reestablished at 2pm. By 5 pm, large industry load starts to shut down and people get off work and back home. There is a peak value of electricity consumption around 6 and 8 pm and then it descends rapidly and reach a minimum value around 2 to 3 am the next day, as most people should be sleeping. The shape of the load curve is presented for 24 hours for every month.

But there are some differences in the daily peak value because of the weather change during the year. Especially, the load demand in summer (June and July) and winter (December, January and February) is a bit higher compared to a similar pattern of lower values during the Spring /Fall (April and September). This feature can be determined easily when observing the load demand curve for a sampling year as shown in Figure 4-10.

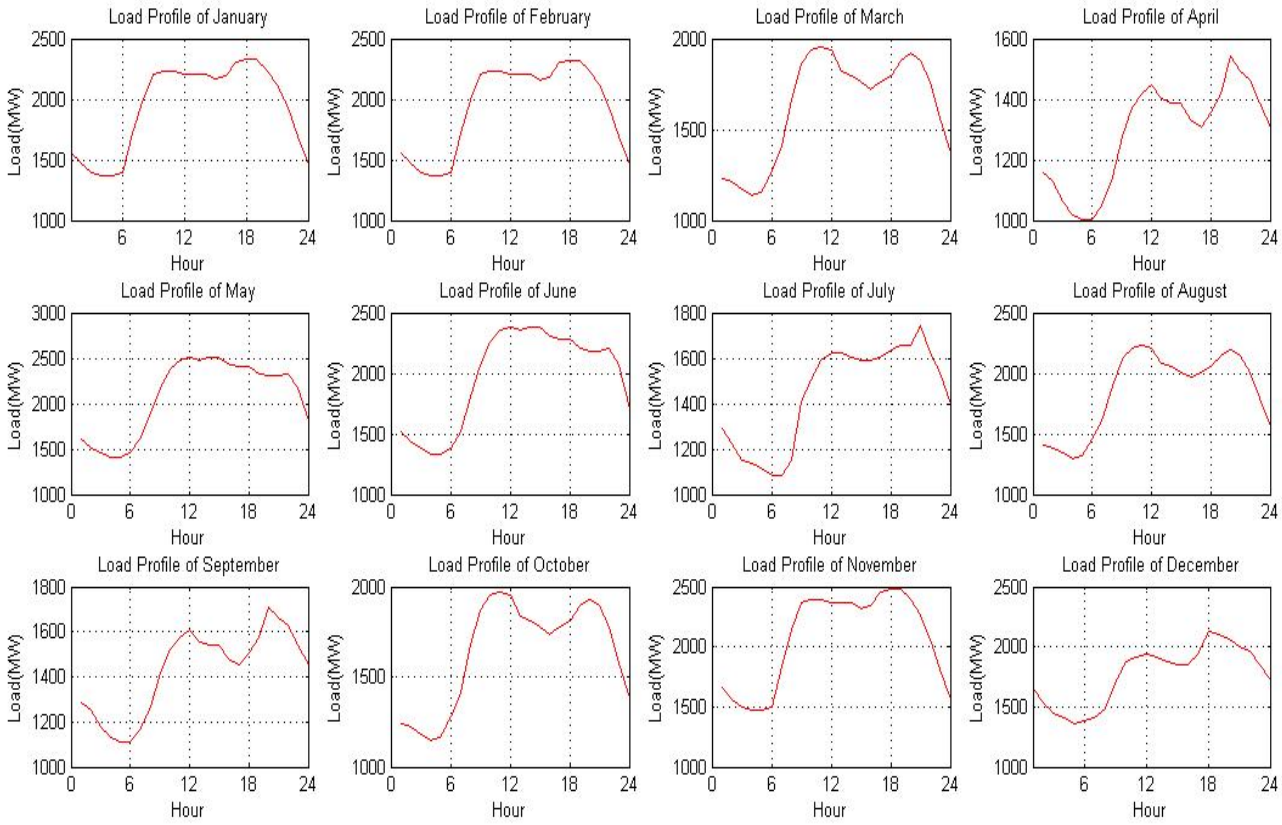

Figure 16. Hourly load profile for 12 months

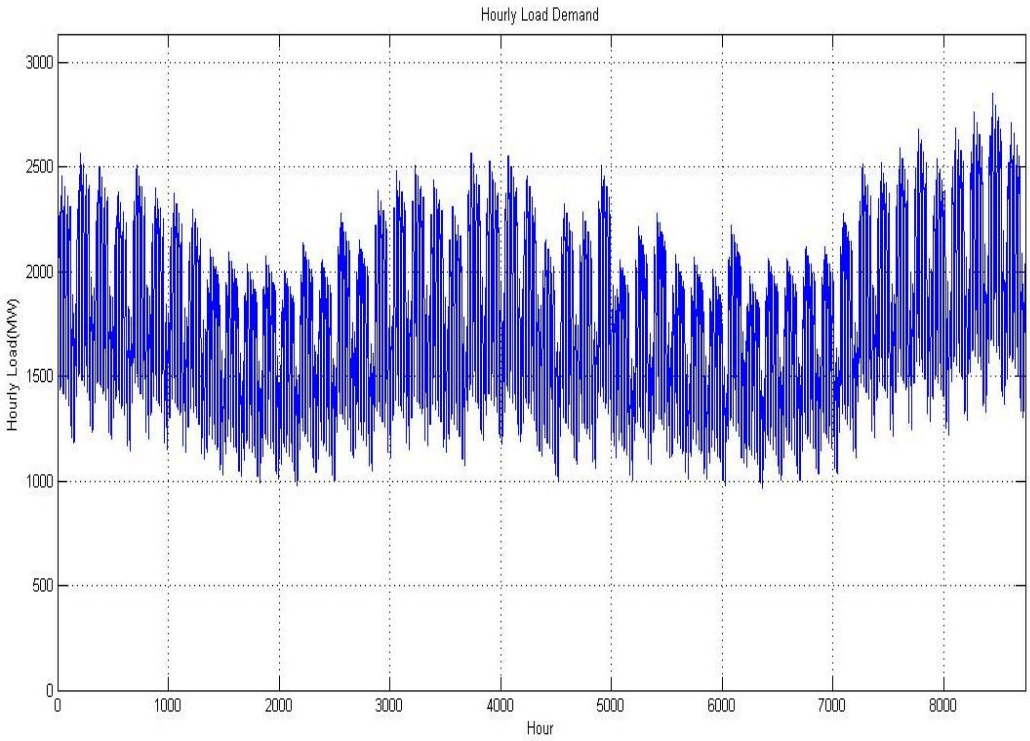

Figure 17. Annual hourly load curve for the IEEE RTS with peak load 2850 MW

4.5 LOLP Assessment Approach

There are some widely used reliability indices based on the conventional system model. In each sampled year, for example in year i, the loss of load duration (LLD_i) in hours, the loss of load occurrence (LLO_i), the energy not supplied (ENS_i), loss of load probability or expectation ($LOLP\ or\ LOLE$) [19]. Among these indices, LOLP is the most widely used probabilistic approach for adequacy assessing of a given network configuration.

A LOLP analysis is typically performed on a system to determine the amount of capacity that needs to be installed to meet the desired reliability target. The calculation involves combining the load profiles and the generator outages with the probability of the generator unexpected breakdown and scheduled outage rates to determine the expected number of hours in the year when a power shortage might occur. LOLP calculation can be obtained hourly and the general principle is to start with a full year of data and calculate the LOLP for this time period. During off-peak periods when there is excess generation capacity available, the LOLP values will usually be zero. Non-zero LOLP values occur when there is shortfall of generation to meet the load. The LOLP evaluation effectively searches for hours or days when there is some risk of not covering the load, discarding the overwhelming majority of hours during which there is little to no risk (LOLE ≈ 0) [23].

In this research, the LOLP is defined as the percentage of number of hours in a year in which the hourly peak load is expected to exceed the available generating capacity, in other words, it is the energy shortage time period divided by the total simulation time therefore can be calculated using the following equation:

$$LOLP = \frac{\sum_{i=1}^{N} LLD_i}{N * 8736} \qquad (4\text{-}13)$$

where

N is the total sampling year (8736 hours/year)

LLD_i is the loss of load duration and is the number of hours when energy deficit (ED) in MWh is positive:

$$ED = L - P_g \qquad (4\text{-}14)$$

P_g is the system available generation capacity in Watt

L is the system hourly peak demanded load in Watt

The availability of generating units is an important factor in capacity adequacy studies. Accurate data in the form of MTTF and MTTR values can be used to conduct evaluation of the system generation adequacy studies. These data are not available for PV units. In this research, PV

panel failure and repair characteristics are simulated by the PV model as described in previous section. The sequential up-down-up cycles of conventional generating units are then combined with the hourly available solar power generated from the PV modules to obtain the final hourly available generation energy of the system [14].

The next step is to obtain the hourly peak load data of the system. As described in the previous section, the annual hourly peak load profile can be derived from the daily/weekly/yearly peak load data.

The last step is to superimpose the system available capacity curve on the chronological hourly load curve to acquire the system margin information. Figure 4-8 is an example of the combination of generating system and load model. In this figure, ENS stands for the energy not supplied. A positive difference represents the system generation is adequate to supply the consumer load, while a negative margin indicates that an energy deficit is occurring [19].

Table B- 1

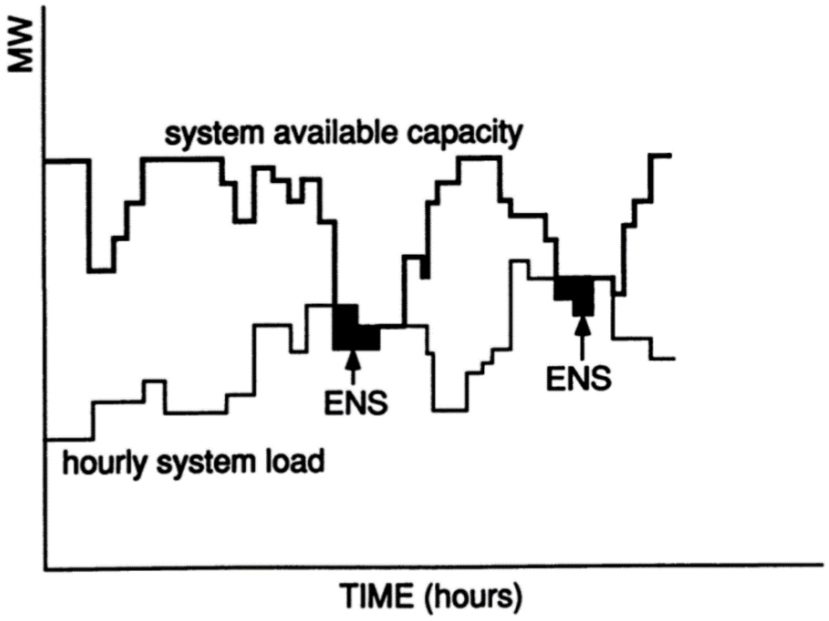

Figure 18. Superimposition of the system available capacity on the load model *[19]*

Chapter 5
System Cost Optimization of Solar PV System

In utility-scale PV system design, it is important to consider both the power generation adequacy level and system security problem. Higher penetration of solar PV generation in a power system means that more diesel units can be superseded by the PV panels, which can save huge cost from the reduction of fuel utilization and the greenhouse gas emissions. However, this action definitely will result in excessive installation cost of PV panels. Meanwhile, higher PV penetration brings up the reliability and security problem. This is because sometimes solar energy output is out of the utilities' control due to the weather conditions and the unavailability during the night time. Consequently, large PV penetration could impose a higher risk of generation adequacy level and could incur additional expenses in the mitigation of network power redistribution. Therefore, there is a competition between the system PV penetration level and the budget constraints. To acquire an equilibrium between cost and reliability requirement, an optimization method is proposed to determine optimum size of a utility-scale PV system based on minimum cost with a satisfactory reliability level.

Cost function model for the utility-scale PV system is constructed in terms of the system capacity. To guarantee the sufficient system generation to avoid severe system energy deficit consequences, the reliability index – LOLP is evaluated to weigh the PV substitution level in the conventional generating system.

In this chapter, the cost of utility-scaled PV system is described in detail in the first section, including the initial capital cost, mitigation cost and the saving fuel cost. A desired LOLP of the system is defined to restrict the maximum acceptable capacity of the utility-scale PV system for the proposed optimization process. And the optimal location of the installation and the appropriate PV displacement ratio is tested.

5.1 System Cost Function

A constrained, single variable optimization problem is formulated as:

$$Minimize_x\ f(x) \qquad (5\text{-}1)$$

subject to the constraint: $x_{min} \le x \le x_{max}$

In this research, the size of the photovoltaic solar energy capacity is the only decision variable, and the total system cost function is fitness function to be minimized.

The estimated system cost function model consists of three parts and can be expressed as:

$$Minimize_{C_{pv}} \{C(C_{pv})\} = min\{C_{in} + C_m - C_s\} \qquad (5\text{-}2)$$

subject to the constraint: $LOLP_{pv} \le LOLP_{pv\_max}$

where

C_{pv} is the utility-scale PV system capacity in Watt

C_{in} is the capital installation cost in $

C_m is the mitigation cost in $

C_s is the saving operation cost in $

Capital Installation Cost of PV system

When installing utility-scale PV systems, the installation techniques are considered to be the best-in-class and the prices of system benchmarks reflects the national averages of the installed capacities. The benchmark of utility systems stands for ground-mounted, fixed-tilt and single-axis tracking systems. The utility-scale system prices are presented in Figure 5-1 [24].

As shown in this figure, the U.S. utility-scale PV system unit price experienced a rapid decrement between 2009 and 2015. In general, the unit cost takes into account: material fees and prices of installation work by participating labors, and other like geographic or environment cost. A reduction of equipment price has been an important inspiration of reduction in overall system cost in recent years. The hardware material category includes such things as PV modules, inverters, racking and all balance-of-system (BOS) hardware requested for a complete system. Expenditure on installation labor seems contribute to a relatively small percentage of the total system prices

when compare to hardware costs and other soft cost sections. Other soft costs remain a significant part of total system price, involving land space control, environmental permitting and interconnection costs [24].

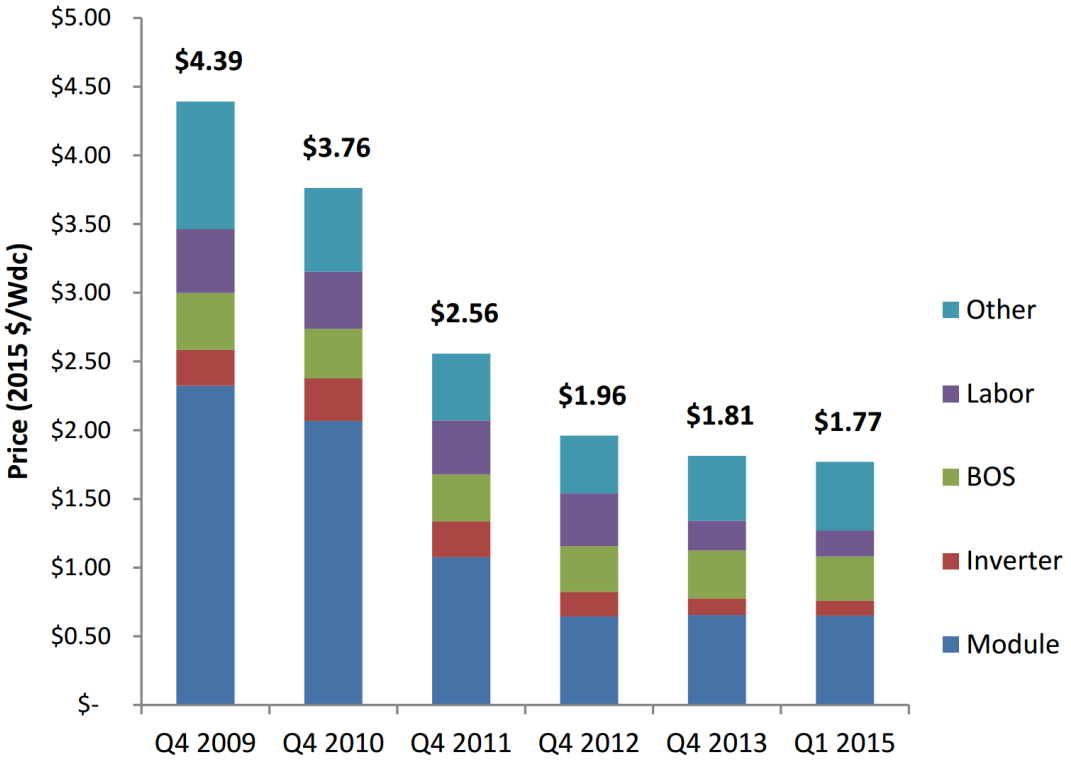

Figure 19. Utility-scale PV installed prices *[24]*

Then, the overall capital cost for utility-scale PV system is indicated to be proportional to its system capacity. Given the system installation price approximately $1.77/W in 2015, the estimated capital investment is calculated using the following formula:

$$C_{in} = C_{pv} * 1.77 \qquad (5\text{-}3)$$

where

C_{pv} is the generation capacity utility-scale PV systems in Watt

Mitigation Cost

When planning a solar PV generation system, the mitigation cost plays a significant role in the estimation of the total expenses. Power engineers are concerned with the protection of the current network configuration and in this regards, they have to predict the potential risk factors or unstable operations due to PV integration in the system. So, the system responses of solar energy injection and absence of some power facilities is examined by the N-1 contingency analysis. The results can provide the system state violations of a specific location.

As discussed in Chapter 3, any interruptions in the system may lead to line overloading and bus voltage collapse. N-1 contingency analysis is expanded with the iterative AC power flow, which provide the operation states. Then bus voltage and power flow along each branch will be examined. The algorithm looks for out-of-limit operation, either power flow exceed the capacity of line or bus voltage drops below the acceptable range and records these violations. Regarding these factors, two types of mitigation measures are implemented to minimize the impacts of contingency:

a) Overload mitigation: a new transmission line is rebuilt where a power line is delivering the amount of power exceeding the allowable maximum power
b) Voltage collapse mitigation: static var compensator (SVC) is placed to supply reactive power to the load bus where voltage collapse occurs.

Commonly, there are always some lines and buses found out violated in different contingency scenarios. To reasonably expect the mitigation cost, only the most severe violation of each bus and line are taken into account and recorded for cost estimation.

Table 5-1 gives the capital cost data of SVC and transmission line for the utility company. Transmission line cost are determined by their voltage rating and proportional to their length in mile. The line operating at higher voltage is more expensive compared to that of the lower voltage line. Meanwhile, the cost of SVC is dependent on the reactive power capacity in MVAR that is required to restore the bus voltage to an acceptable level and the determination of the required reactive power capacity is referred to the Q-V analysis as described in Chapter 3.

$$C_m = \sum_{i=1}^{k} C_{line} \times L_{line} + \sum_{m=1}^{n} C_{SVC} \times Q \qquad (5\text{-}4)$$

where

C_{line} is the unit cost of line in $

C_{SVC} is the unit cost of SVC in $/MVAr

L_{line} is the length of transmission line in mile

Q is the reactive power capacity in MVAr

Table 5-1. Capital cost data of SVC and transmission line

Description	Voltage (kV)	Unit	Unit Cost (Millions)
Transmission line	230	Per mile	$1.5
Transmission line	138	Per mile	$1.0
Static Var Comp(SVC)	All	Per 10 MVAR	$ 25

Saving Generation Cost

To estimate the saving cost of solar PV power generation stations taking the place of fuel burning ones, the fundamental idea is to know the capacity of fuel-burning power facilities that is replaced by PV power.

Regarding to the power balance in the system, a number of conventional generators will be replaced and shut down when the solar power is injected. The capability of the PV system to replace the conventional generation is calculated with the PV system's displacement ratio using the formula:

$$C_{re} = C_{pv} \times R_{re} \quad (5\text{-}5)$$

where

R_{re} is defined as the replacement ratio

C_{re} is the size of unit displaced by PV system

For example, if the PV system is sized at 100MW and the displacement ration is 80%, the replaced conventional unit size is around 80 MW and the rest of the power injection from other generators will be reduced by 20 MW automatically when running the power flow program.

When determine the replaced conventional generator, the Operation & Maintenance Cost (O&M cost) data will be used for reference. From the environmental and economic perspective, the ones with higher O&M will be shut down first.

The estimated operation time for the shut-down unit can be obtained with the forced outage rates and scheduled maintenance data,

$$T = (8760 - 24 \times 7 \times SMT) \times (1 - FOR) \quad (5\text{-}6)$$

where

SMT is the scheduled maintenance time in weeks/yr.

FOR is the forced outage rates in percentage

Assume the conventional generating facility can operate with full capacity output, so the expected electricity generation from a displaced generator is

$$P_{re} = T \times C_{gen} \quad (5\text{-}7)$$

where

P_{re} is the expected electricity generation capacity of the displaced generator in MWh

C_{gen} is the generator capacity in MW

Then, the O&M cost data consisting of fixed cost in $/kW/yr and variable cost in $/MWh can be used for saving cost calculation for each generating unit.

For a 25-year round solar PV system, its saving cost due to the PV displacing fossil fuel generation can be obtained by:

$$OC = [FC \times C_{gen} \times 10^3 + VC \times GC] \times 25 \quad (5\text{-}8)$$

where

FC is the fixed cost of the O&M cost in $/kW/yr

VC is the variable cost of the O&M cost in $/MWh

Figure 5-2 shows the generating unit operation data of RTS data, and this will be used for the proposed method in this research.

Table 5-2. Generating Unit Operation Cost Data *[19]*

Size MW	Type	Fuel	Output %	Heat rate Btu/kWh	O&M cost Fixed $/kW/yr	O&M cost Variable $/MWh
12	Fossil steam	#6 oil	20	15600	10.0	0.90
			50	12900		
			80	11900		
			100	12000		
20	Combus. turbine	#2 oil	80	15000	0.30	5.00
			100	14500		
50	Hydro					
76	Fossil steam	coal	20	15600	10.0	0.90
			50	12900		
			80	11900		
			100	12000		
100	Fossil steam	#6 oil	25	13000	8.5	0.80
			55	10600		
			80	10100		
			100	10000		
155	Fossil steam	coal	35	11200	7.0	0.80
			60	10100		
			80	9800		
			100	9700		
197	Fossil steam	#6 oil	35	10750	5.0	0.70
			60	9850		
			80	9840		
			100	9600		
350	Fossil steam	coal	40	10200	4.5	0.70
			65	9600		
			80	9500		
			100	9500		
400	Nuclear steam	LWR	25	12550	5.0	0.30
			50	10825		
			80	10170		
			100	10000		

5.2 System Constraints Conditions

The proposed optimization process has a constraint condition to achieve an optimum value. The reliability index – LOLP is used as the constraint to set the limitation of variable PV system capacity.

From a previously defined LOLP, the capacity range can be calculated using the MCS in Chapter 4. Therefore, each value of PV system size will induce different values of LOLP, which can help to construct the variable C_{pv} limit.

As the optimization constraint condition, the LOLP limitation is applied to set the maximum allowable PV system capacity C_{pv_max}. In this case, it is assumed that the utility company considers that the system energy generation is efficient and defined as acceptable adequacy level when LOLP is lower than 0.2%. Therefore, the maximum value of utility-scale PV system capacity C_{pv_max} can be determined based on large amount of LOLP simulation results. Applying the capacity limits, the PV size optimization problem can be rewritten as

$$Minimize_{C_{pv}} \{C(C_{pv})\} = min\{C_C + M_C + O_C\} \quad (5\text{-}9)$$

subject to the constraint: $1 \leq C_{pv} \leq \mathrm{C}_{pv\_max}$

Note: the utility-scale PV system is defined as the ones with solar generation capacity of 1 MW or more, so the C_{pv_min} is set to 1 MW.

Chapter 6
Simulation Results and Analysis

6.1 Solar Power Output

The proposed approach for optimizing PV system capacity has been applied to the design of a utility-scale PV system in the IEEE-RTS system using solar radiation data from a site located in the state of Virginia, U.S with geographical coordinates defined as:

Latitude: 36.9º Longitude: -76.2º Elevation: 7ft above sea level

The solar irradiation data in long term is possessed on NREL website for the Norfolk, VA between the year 1978 and 1990 [20]. The solar data elements measured and recorded by the NREL includes global horizontal irradiance (GHI), direct normal irradiance (DNI), diffuse horizontal irradiance (DHI), and global horizontal illuminance. In this thesis, the global radiation (GHI) is used for study. The sample time of the data is 1 hour, so there are 24 samples value per day, and a total of 8736 data for a sampling year. The hourly solar radiation data in W/m^2 for the simulation are attached in Appendix A. Figure 6-1 shows the plots of solar PV energy output versus time for a year.

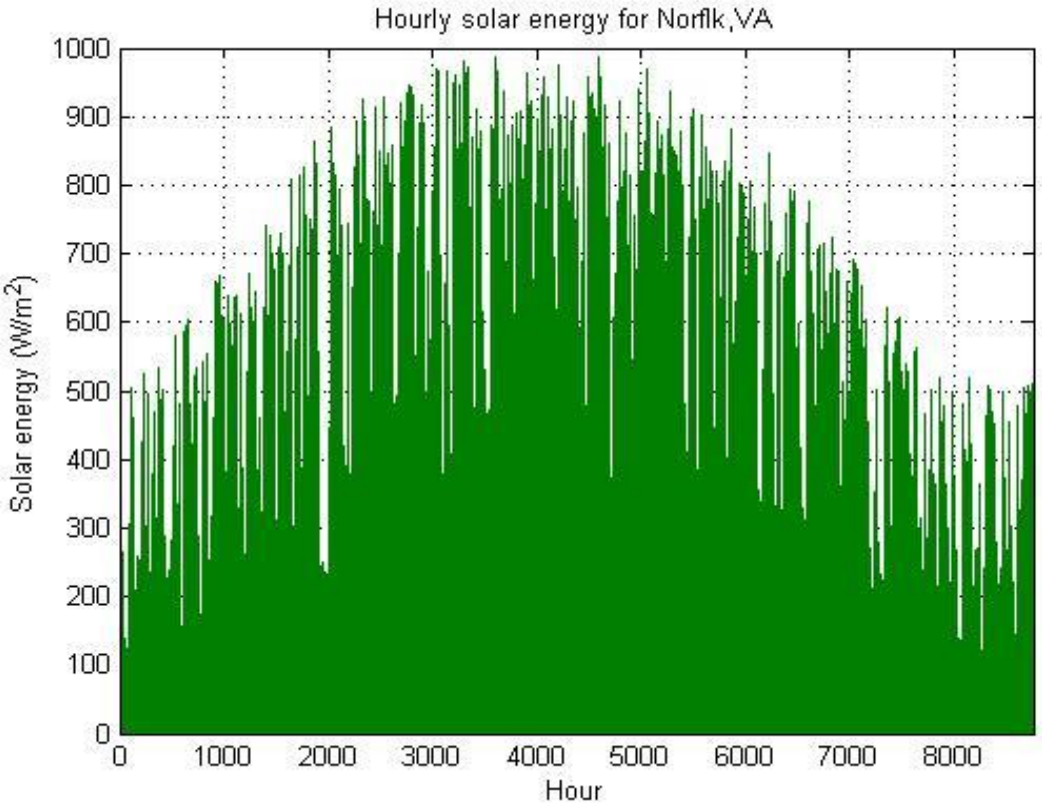

Figure 20. Hourly irradiation for Norfolk, Virginia *[20]*

As described in Chapter 4, solar energy output can be estimated with the irradiation data by using the Equation 4-11. Some system parameters are specified initially to define the characteristics of the equipment. Regarding to the latest PV generation technology, PV module's efficiency is close to 22%, inverter's efficiency is up to 85%, the connection and wiring efficiency is around 95%. Therefore, the solar energy output of the system can be determined by the area of PV modules.

6.2 LOLP with Solar PV Penetration

The IEEE RTS has Bus 13 referred as the slack bus, 10 voltage-controlled buses (1, 2, 7, 14 to 16, 18, and 21 to 23) and the rest (13 buses) are load buses. There are 32 generators ranging from 12 MW to 400 MW involved in this system. The annual load curve consists of 8736 hourly load points. The full details of the RTS can be found in Appendix C "IEEE RELIABILITY TEST SYSTEM".

The system available capacity is obtained by combining the operating cycles of all the units. Figure 6-2 shows the system available capacity model in a typical sample year. The total installed capacity in the system is 3405 MW. The annual load model for the IEEE RTS is demonstrated in Figure 4-9 in Chapter 4. The annual peak load for the test system is 2850 MW.

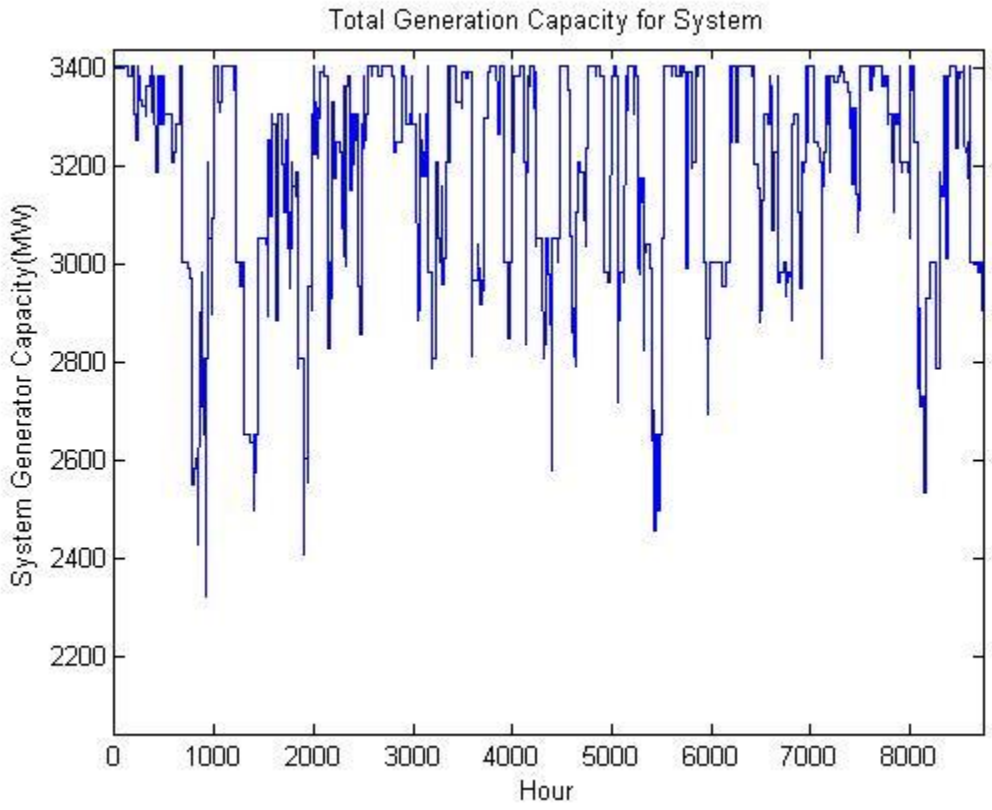

Figure 21. System Available capacity in a sample year

Figure 6-3 shows the evaluated reliability index of LOLP for different capacity of PV generation installation with 80% displacement ratio. Each curve is generated by applying the Monte Carlo Simulation with state duration curve. These results are for 1500 sampling years and these curves demonstrate the convergence processes of the LOLP index, respectively, as the number of sampling year goes up. It can be noted that the LOLP index of the green curve (20MW PV system) appears to have lowest risk of loss the load (LOLP = 0.12%), while the red curve of 80 MW-PV system has the highest possibility to power shortage (LOLP = 0.17%).

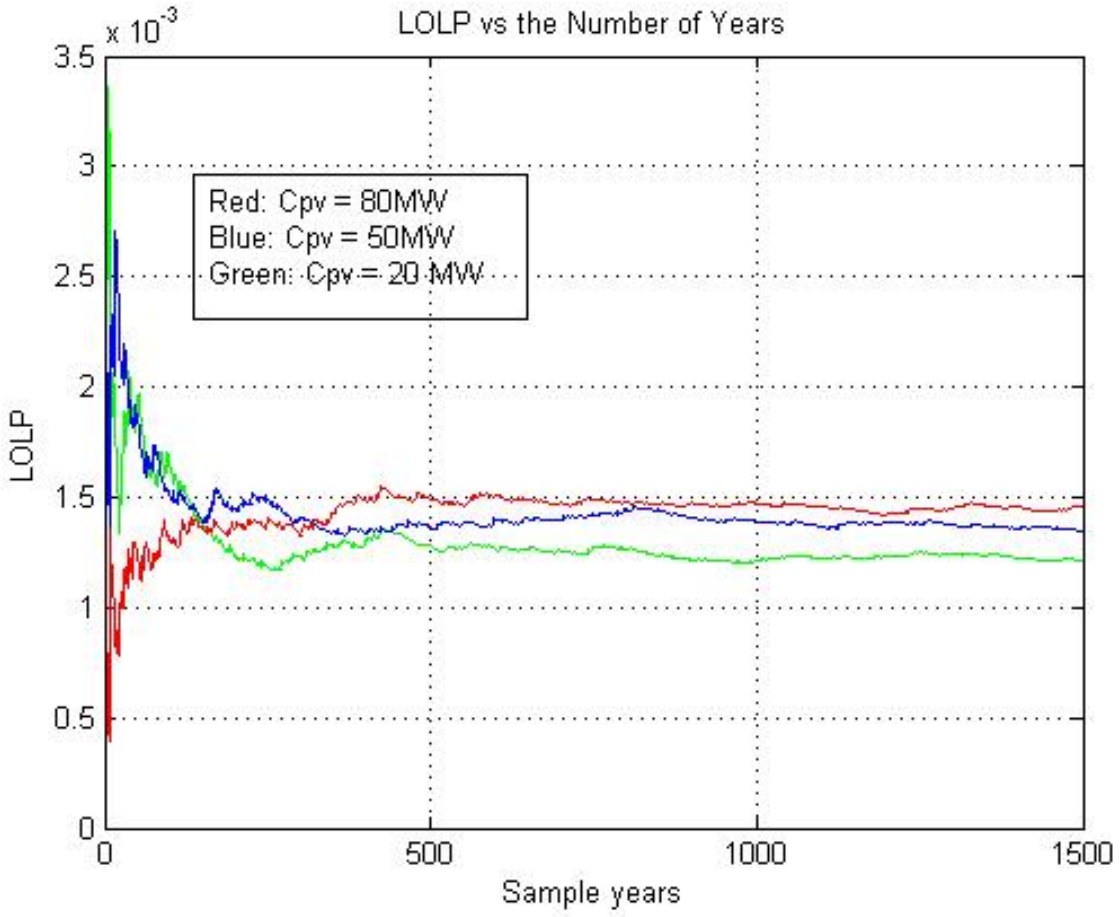

Figure 22. LOLP with different solar PV capacity at 80% replacement ratio

Figure 6-4 shows the trend of the LOLP with different PV system capacity in the range of [20, 140] at 80% displacement ratio. When progressively increase solar PV generation in system, the LOLP value is continuously increasing which presents an incremental risk of energy deficit and system failure. It can be seen that increased solar PV penetration will lower the reliability level of the entire system.

When different PV capacity is installed in the system, the number of conventional generating units in system changes because some units can be replaced by PV generation system. Table 6-1 lists the system changes with different PV capacity. The system with a higher PV generation, which displaces more conventional generation in the form of diesel units does not improve the system generation adequacy level. This is due to the fact that the PV units generate very little or no energy during the night time. The primary benefit with higher PV generation is the reduction in the significant cost of diesel fuel that was once required to supply the load.

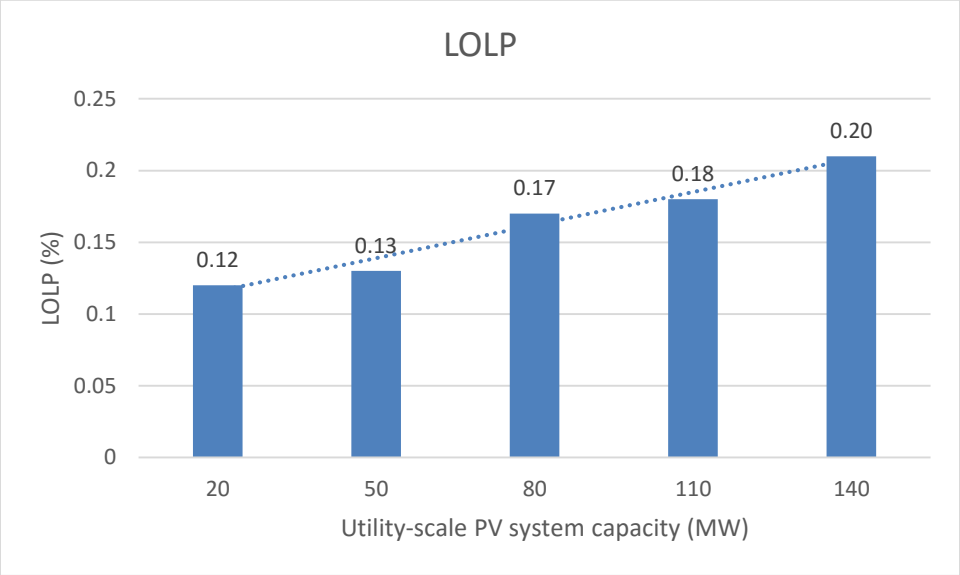

Figure 23. LOLP for different capacity of solar PV system

Table 6-1. System Configuration Changes

PV System Capacity	Displacement Ratio	Displaced Capacity	Off_12 Unit	Off_20 Unit	LOLP
20 MW	80%	16 MW	1	0	0.12%
50 MW	80%	40 MW	0	2	0.13%
80 MW	80%	64 MW	0	3	0.17%
110 MW	80%	88 MW	0	4	0.18%
140 MW	80%	112 MW	2	4	0.20%

Note: In this table, Off_12 Unit and Off_20 Unit are the number of 12 MW and 20 MW generating units substituted by PV generation, correspondingly.

Assume the system is required to meet the desired reliability target, commonly expressed as an expected LOLP of 0.2%. With a large amount of LOLP simulation results for different capacity of PV systems, the constraint of cost function can analytically verify that the maximum allowable PV system capacity is 140 MW. Therefore, the function constraint can be simplified as an explicit variable constraint and the optimization problem can be expressed as:

$$Minimize_{C_{pv}} \{C(C_{pv})\} = min\{C_{in} + C_m - C_s\} \quad (6\text{-}1)$$

subject to the constraint: $1 \leq C_{pv} \leq 140$

6.3 Contingency Analysis Simulation

To check the security problem of integrating PV system with the original system, N-1 contingency analysis is expanded to look for the locations or component of potential risk. As demonstrated in Chapter 3, the N-1 contingency analysis with single line outages is tested on an IEEE RTS, which has 24 Bus, 38 Branch. Therefore, thirty-eight single line outage contingency circumstances are simulated.

For example, the N-1 analysis is formed when a 60-MW PV system is installed on Bus 5. Table 6-2 shows the line flow violations that line power exceeds its MVA emergency rating. Table 6-3 shows the bus voltage collapse results.

Table 6-2. Line Overloading Results with Single Line Outage

Contingency Line No.	From Bus	To Bus	V rate (kV)	Length (mile)	MVA rate	MVA Overloading
5	2	6	138	50	220	237.43
10	6	10	138	16	200	308.98

Table 6-3. Voltage Collapse Results with Single Line Outage

Contingency Bus No.	Base voltage (kV)	Q demand (MVAR)	V_max (p.u.)	V_min (p.u.)	V violation (p.u.)
3	138	28	1.05	0.95	0.9264
6	138	37	1.05	0.95	0.6733

Given the PV installation bus location and the PV size, group of N-1 contingency analysis are expanded. Among all those contingency cases, Line 5 and 10 always have trouble with power flow when one transmission line is taken out of service, so the solution is to reconstruct new lines correspondingly to satisfy the continuous and secured power supply. Referring to the system diagram, it can be noted that Bus 6 is connected to the system with only two branches, which are just the risk branch Line 5, from Bus 2 to Bus 6, and Line 10, from Bus 6 to Bus 10. Therefore, to ensure the power is transferred to Bus 6, each one of these two branches is out of service, another branch could be overloaded.

As for the bus voltage violation, the analysis finds out Bus 3 and Bus 6 are the most unstable locations where the voltage collapse phenomenon commonly takes place in different contingency case.

According to the system bus information, Bus 3 is essentially heavily loaded compared to most of the others. This bus is connected to Bus 1, 9 and 24, that Bus 1 has the small-sized

generators range from 20 MW to 76 MW that will be shut off and replaced by PV system sometimes and contributes small amount of power to Bus 3 and both Bus 9 and 24 have no power injections at all. That makes the overall power supply to Bus 3 is not guaranteed and consequently result power insufficient and voltage collapse.

As for Bus 6, it has heavy load demand on bus as well. The connected neighboring buses are Bus 2 and 10, that Bus 2 has the smallest generators (20 MW and 76 MW) which could be replaced by PV and Bus 10 has no generator to support the load directly. With regards to those facts, it can be see that these two bus are stressfully loaded in the system and that is why the voltage collapse always happens.

In regard to the violation results, necessary actions can be implemented to keep the power system secure and reliable. The mitigation cost related to voltage control is reactive power compensation and the reactive power capacity is typically estimated by QV curve following general step described in chapter 4. For a line flow overloading, the cost to rebuild a line is a function of the length of the line. Table 6-4 and 6-5 shows the mitigation cost corresponding to violation cases in Table 6-2 and 6-3.

Table 6-4. Mitigation Cost of Line Reconstruction

Contingency Line No.	From Bus	To Bus	V rate (kV)	Length (mile)	Cost (Million)
5	2	6	138	50	$50
10	6	10	138	16	$16

Table 6-5. Mitigation Cost of Reactive Power Compensation

Contingency Bus No.	Base voltage (kV)	Compensation (MVAr)	Violated Voltage (p.u.)	Regulated Voltage (p.u.)	Cost (Million)
3	138	57	0.92	0.98	$150
6	138	132	0.67	0.95	$325

6.4 Cost Optimization Results

To optimization process is accomplished in the generic algorithm (GA) optimization toolbox in MATLAB directly. The convergence process to the global optimum solution of the proposed optimization model has been verified by changing the PV size in the process and calculating corresponding system cost. This procedure is repeated for every bus location in the system. The optimal sizing results, considering all 24 bus to be the candidate PV system location with three displacement ratios are shown in Table 6-6.

The optimal sizing results consists of the optimal bus number, optimal PV capacity, and the cost information in detail. For the different displacement ratio, it can be noted that the mitigation cost has been a significant portion of the total system cost and the best PV system capacity is around 59 MW. The variation of the total system cost during the optimization process indicates that the total system cost with 80% displacement ratio is the lowest compared to those of 50% and 30% displacement ratio. This is due to the higher saving of fuel cost.

Comparing these solutions of different displacement plans, Bus 3 always has the minimum mitigation cost, which makes it the best location for the PV installation. It should be noted that Bus 3 has been a potential risk location of voltage collapse due to its heavily load demand. It is the installation of solar PV system on Bus 3 that contribute to the power adequacy level of this stressfully loaded bus and efficiently avoid the potential voltage collapse problems.

Table 6-6. Optimization Results

Displace Ratio	Optimal Bus	Optimal PV (MW)	Displace Generation (MW)	Off_12 Unit	Off_20 Unit	Capital Cost (Millions)	Mitigation Cost (Millions)	Fuel Saving (Millions)	Total Cost (Millions)
80%	3	59	47.2	0	2	$104.4	$391	$38.20	$457.2
50%	3	58	29	0	1	$104.4	$391	$19.05	$476.4
30%	3	57	17.1	1	0	$102.6	$391	$5.22	$488.4

Chapter 7
Conclusions and Future Work

7.1 Summary

In this work, a sizing optimization methodology of PV system has been presented to overcome the limitations associated with power system operation and planning. The cost of PV penetration is no longer just PV installation cost, but also includes the system cost due to their impacts on system efficiency and reliability as grids become more complex and unpredictable and operate closer to their limits. With regards to system limits, a new optimization problem formulation was developed together with the assessment of system performance and reliability level.

The two major aspects in designing the size of a utility-scale PV system are:

a) ***Reliability level.*** As described in Chapter 4, the reliability evaluation of LOLP of the system is applied in this work. It is accomplished by predicting the generator performance with the MTTF and MTTR data of a two-state generator model. The Monte Carlo Simulation with state duration method is presented to simulate the performance of the entire system and estimate the system generation capacity. Chronological hourly varying load model is also yielded to characterize the system peak load condition at different season conditions.

b) ***The total system cost.*** A novel and practical model of the total system cost is presented which consists of installation, mitigation cost and fuel saving. The installation cost is only depends on the size of the PV system capacity. The N-1 contingency analysis with AC power flow as described in Chapter 3 analytically shows the mitigation cost corresponding to voltage collapse and line overload circumstances. The π-equivalent transmission line model is used to solve the power flow on specific branch in the system to test the line overload contingency. For mitigation measurement of voltage collapse, the method of QV analysis is used to estimate the reactive power compensation. The fuel cost saving of the entire network is proposed due to the replacement of conventional generating units during a 25-year operation of a PV system. The priority of the shutting down units is determined by their operation & maintenance cost, that is, PV will displace

the most expensive generating units first. Considering different displacement ratio conditions, the corresponding solution of the units' displacement yields various system configurations.

Given the above factors, the optimum capacity of the PV system is determined such that the total system cost is minimized subject to the constraint of LOLP requirement. The minimization process is completed with Genetic Algorithm (GA) toolbox in MATLAB.

The results of reliability evaluation of LOLP verify that the Monte Carlo Simulation with state duration method is a very practical tool to study the performance of the system. It can be seen that higher capacity of PV generation in system gives rise to the risk of losing the load due to its nature of unavailability during night time. Nevertheless, it can replace more conventional generating units. The limit of the reliability level of the system generation is the constraint of PV system capacity C_{pv}, the optimization variable. The main problem in the computation of LOLP-based constraint is to simulate a long period which becomes a time-consuming iteration process. To find an explicit expression of optimization variable constraint, the maximum permissible PV capacity of the system corresponding to the maximum LOLP constraint is determined and directly written in the originally proposed optimization problem model. Therefore, the proposed optimization model has the capacity constraint $C_{pv} \leq C_{pv\_max}$ instead of $LOLP_{pv} \leq LOLP_{pv\_max}$. The corresponding constraint value C_{pv_max} is iteratively computed by performing the LOLP evaluation based on Monte Carlo Simulation. The main advantages of the optimization model with specific constraint of C_{pv} is that it is easy to implement using the mathematical programing tools and that there is no need for computation of the LOLP constraint during the solution process. These advantages result in a more applicable model.

To solve the total system cost, both installation cost and fuel saving will increase as additional PV system are installed. As for mitigation cost, the N-1 contingency methodology is expanded to handle different contingency scenario analysis. The results of every iterative AC power flow provide system operation information and the system violations are examined based on these data such as bus voltage magnitude and power injection. In different contingency scenarios, there are always some lines and buses found out violated. To reasonably expect the mitigation cost, only the most severe violation of each bus and line are taken into account and recorded for cost estimation.

The proposed size optimization method is applied to a test system of 24 buses and up to 32 generating units to study its performance and demonstrate its practical application in realistic

systems. It is noticeable that Bus 3 is the best location for PV system installation with different displacement ratio compared to the other locations in the system. Among all those contingency cases, Line 5 and 10 always have trouble with power flow when one transmission line is taken out of service, so the solution is to reconstruct new lines correspondingly to satisfy the continuous and secured power supply. As for the bus voltage violation, the algorithm finds out Bus 3 and Bus 6 are the most unstable locations where the voltage collapse phenomenon takes place in different contingency case. According to the system information, Bus 3 is relatively heavier loaded compared to most of the others. What's more, the Bus 3 is connected to Bus 1, 9 and 24, where Bus 1 has the smallest generators that will be shut off and replaced by PV system, and both Bus 9 and 24 have no power injections at all. That means the power supply to Bus 3 is not guaranteed to cover the load. As for Bus 6, it is heavily loaded as well and the connected neighboring bus are Bus 2 where has the smallest generator to be replaced by PV and Bus 10 where has no generator to support the load directly. With regards to those facts, it can be noted that these two bus are stressfully loaded in the system. This can properly justify that Bus 3 has been the optimal bus location for the PV installation: the solar PV power injected on this bus can supply the bus load directly and avoid the potential voltage collapse problem efficiently.

7.2 Contributions

The main contributions of this thesis to the field of power engineering are:

1. A theoretical background that supports the use of the Reliability Evaluation to determine the generation adequacy level of a power system has been developed. This is accomplished by using Monte Carlo Simulation with state duration method to predict the generation capacity and potential energy deficit conditions.
2. A novel and practical optimization model of the system, where the PV will be penetrated, is presented. The fitness function of system cost incorporates initial installation cost, potential mitigation cost and future fuel saving. Contingency analysis is utilized to determine the potential operation risk of the system and to get a more comprehensive view of the future performance of the system with PV penetration.
3. It is analytically shown that this method can be used to find out the optimal bus location for the PV in the system.

7.3 Future Work

In this research, it is a regret that the environmental cost data is not available for the cost function model. For the future research, it is reasonable to take into account the environmental pollution cost paid by the utility company due to the greenhouse emissions of diesel generators. With PV displacing the conventional generating units, it can reduce the emission of greenhouse gases, which can save the utility company a large amount of environmental expenditure. After this cost gets involved in the optimization, the results could be more practical and applicable in real case.

Another main disadvantage of the proposed method is the ideal PV model. This model does not take into consideration the outage probability of the PV modules due to maintenance or unexpected breakdown. For future research, the PV model can be specified with more reliability data for more realistic estimation.

Also in this work, PV system is defined to provide only real power to grid. In fact, power electronics engineers are working on invertors that can help PV system to output reactive power. Since PV system is unable to work during night time, it can be used to supply reactive power to system to meet the peak electric energy at night demand in the future.

When considering the priority order of replacing conventional units by solar PV system, the spinning reserve and response time of each unit can be taken into consideration if these starting up time is available for each unit in the system. Because if there is any situation that the solar PV system is not able to generate electricity, the replaced units must start up as soon as possible to generate electricity to support the load.

Appendix A
SOLAR IRRADIATION DATA

A typical meteorological year (TMY) data set provides a reasonably sized annual data set that holds hourly meteorological values that typify conditions at a specific location over a longer period of time. TMY data have natural diurnal and seasonal variations and represent a year of typical climatic conditions for a location. The data set consists of 12 typical meteorological months (January through December) and these monthly data sets contain actual time-series meteorological measurements and modeled solar values.

The TMY data has been released by the National Renewable Energy Laboratory (NREL) in 1994 and can be accessed via the Web: http://rredc.nrel.gov/solar/old_data/nsrdb/1991-2005/tmy3/.

Appendix B

MATPOWER DATA FILE FORMAT

The details of the MATPOWER case format are listed in the tables below.

Table B1. Bus Data (mpc.bus)

name	column	description
BUS_I	1	bus number (positive integer)
BUS_TYPE	2	bus type (1 = PQ, 2 = PV, 3 = ref, 4 = isolated)
PD	3	real power demand (MW)
QD	4	reactive power demand (MVAr)
GS	5	shunt conductance (MW demanded at $V = 1.0$ p.u.)
BS	6	shunt susceptance (MVAr injected at $V = 1.0$ p.u.)
BUS_AREA	7	area number (positive integer)
VM	8	voltage magnitude (p.u.)
VA	9	voltage angle (degrees)
BASE_KV	10	base voltage (kV)
ZONE	11	loss zone (positive integer)
VMAX	12	maximum voltage magnitude (p.u.)
VMIN	13	minimum voltage magnitude (p.u.)
LAM_P†	14	Lagrange multiplier on real power mismatch (u/MW)
LAM_Q†	15	Lagrange multiplier on reactive power mismatch (u/MVAr)
MU_VMAX†	16	Kuhn-Tucker multiplier on upper voltage limit (u/p.u.)
MU_VMIN†	17	Kuhn-Tucker multiplier on lower voltage limit (u/p.u.)

† Included in OPF output, typically not included (or ignored) in input matrix. Here we assume the objective function has units u.

Table B2. Generator Data (mpc.gen)

name	column	description
GEN_BUS	1	bus number
PG	2	real power output (MW)
QG	3	reactive power output (MVAr)
QMAX	4	maximum reactive power output (MVAr)
QMIN	5	minimum reactive power output (MVAr)
VG	6	voltage magnitude setpoint (p.u.)
MBASE	7	total MVA base of machine, defaults to baseMVA
GEN_STATUS	8	machine status, > 0 = machine in-service; ≤ 0 = machine out-of-service
PMAX	9	maximum real power output (MW)
PMIN	10	minimum real power output (MW)
PC1*	11	lower real power output of PQ capability curve (MW)
PC2*	12	upper real power output of PQ capability curve (MW)
QC1MIN*	13	minimum reactive power output at PC1 (MVAr)
QC1MAX*	14	maximum reactive power output at PC1 (MVAr)
QC2MIN*	15	minimum reactive power output at PC2 (MVAr)
QC2MAX*	16	maximum reactive power output at PC2 (MVAr)
RAMP_AGC*	17	ramp rate for load following/AGC (MW/min)
RAMP_10*	18	ramp rate for 10 minute reserves (MW)
RAMP_30*	19	ramp rate for 30 minute reserves (MW)
RAMP_Q*	20	ramp rate for reactive power (2 sec timescale) (MVAr/min)
APF*	21	area participation factor
MU_PMAX†	22	Kuhn-Tucker multiplier on upper P_g limit (u/MW)
MU_PMIN†	23	Kuhn-Tucker multiplier on lower P_g limit (u/MW)
MU_QMAX†	24	Kuhn-Tucker multiplier on upper Q_g limit (u/MVAr)
MU_QMIN†	25	Kuhn-Tucker multiplier on lower Q_g limit (u/MVAr)

* Not included in version 1 case format.
† Included in OPF output, typically not included (or ignored) in input matrix. Here we assume the objective function has units u.

Table B3. Branch Data (mpc.branch)

name	column	description
F_BUS	1	"from" bus number
T_BUS	2	"to" bus number
BR_R	3	resistance (p.u.)
BR_X	4	reactance (p.u.)
BR_B	5	total line charging susceptance (p.u.)
RATE_A	6	MVA rating A (long term rating)
RATE_B	7	MVA rating B (short term rating)
RATE_C	8	MVA rating C (emergency rating)
TAP	9	transformer off nominal turns ratio, (taps at "from" bus, impedance at "to" bus, i.e. if $r = x = 0$, $tap = \frac{\lvert V_f \rvert}{\lvert V_t \rvert}$)
SHIFT	10	transformer phase shift angle (degrees), positive ⇒ delay
BR_STATUS	11	initial branch status, 1 = in-service, 0 = out-of-service
ANGMIN*	12	minimum angle difference, $\theta_f - \theta_t$ (degrees)
ANGMAX*	13	maximum angle difference, $\theta_f - \theta_t$ (degrees)
PF†	14	real power injected at "from" bus end (MW)
QF†	15	reactive power injected at "from" bus end (MVAr)
PT†	16	real power injected at "to" bus end (MW)
QT†	17	reactive power injected at "to" bus end (MVAr)
MU_SF‡	18	Kuhn-Tucker multiplier on MVA limit at "from" bus (u/MVA)
MU_ST‡	19	Kuhn-Tucker multiplier on MVA limit at "to" bus (u/MVA)
MU_ANGMIN‡	20	Kuhn-Tucker multiplier lower angle difference limit (u/degree)
MU_ANGMAX‡	21	Kuhn-Tucker multiplier upper angle difference limit (u/degree)

* Not included in version 1 case format. The voltage angle difference is taken to be unbounded below if ANGMIN < -360 and unbounded above if ANGMAX > 360. If both parameters are zero, the voltage angle difference is unconstrained.

† Included in power flow and OPF output, ignored on input.

‡ Included in OPF output, typically not included (or ignored) in input matrix. Here we assume the objective function has units u.

Appendix C
IEEE RELIABILITY TEST SYSTEM

Network Configuration

The IEEE Reliability Test System (RTS) was developed by the Subcommittee on the Application of Probability Methods in the IEEE Power Engineering Society [19]. This system consists of 24 bus connected by 38 lines and transformers, as shown in Figure C-1.

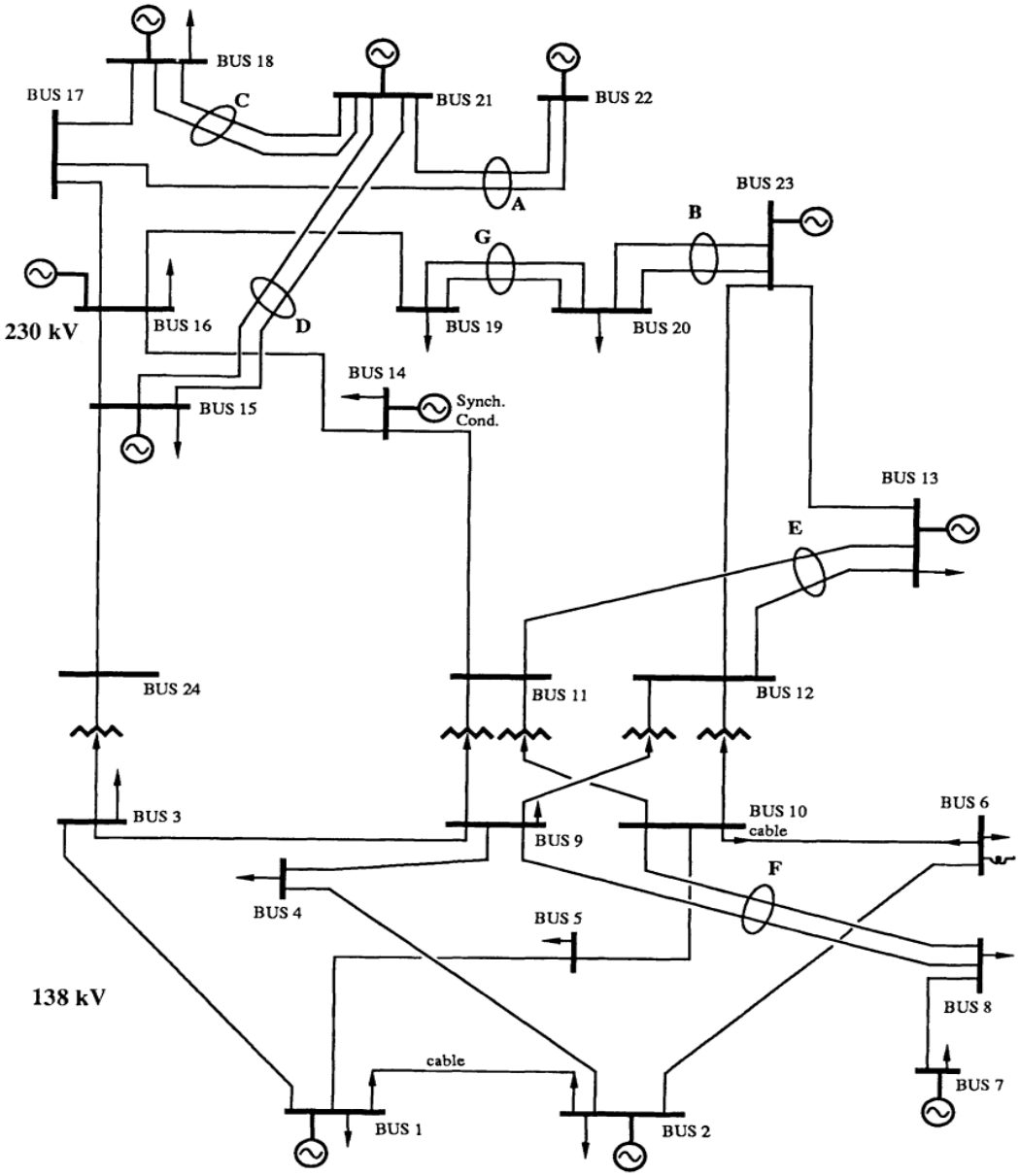

Figure C-1. IEEE RTS system diagram

Transmission System Data

The transmission lines are at two voltages, 138 kV and 230 kV. The 230-kV area is at the top part of the network, with 230/138 kV substations at Buses 11, 12 and 24. The locations of the generating units are lists in Table C1. The system has voltage corrective devices at Bus 14 (synchronous condenser) and Bus 6 (reactor). Table C2 shows data on generating unit MVAr capacities. The bus load data at the time of system peak are shown in Table C3. Transmission line length and forced outage data are presented in Table C4.

Table C1. Generating Unit Locations

Bus	Unit 1 MW	Unit 2 MW	Unit 3 MW	Unit 4 MW	Unit 5 MW	Unit 6 MW
1	20	20	76	76		
2	20	20	76	76		
7	100	100	100			
13	197	197	197			
15	12	12	12	12	12	155
16	155					
18	400					
21	400					
22	50	50	50	50	50	50
23	155	155	350			

Table C2. Generating Unit MVAr Capacities

Size (MW)	MVAr	
	Minimum	Maximum
12	0	6
20	0	10
50	−10	16
76	−25	30
100	0	60
155	−50	80
197	0	80
350	−25	150
400	−50	200

Table C3. Bus Load Data

	Load	
Bus	MW	MVAr
1	108	22
2	97	20
3	180	37
4	74	15
5	71	14
6	136	28
7	125	25
8	171	35
9	175	36
10	195	40
13	265	54
14	194	39
15	317	64
16	100	20
18	333	68
19	181	37
20	128	26
Total	2850	580

Table C4. Transmission Line Length and Forced Outage Data

			Permanent		Transient
From bus	To bus	Length miles	Outage rate 1/yr	Outage duration hr	Outage rate 1/yr
1	2	3	.24	16	0.0
1	3	55	.51	10	2.9
1	5	22	.33	10	1.2
2	4	33	.39	10	1.7
2	6	50	.48	10	2.6
3	9	31	.38	10	1.6
3	24	0	.02	768	0.0
4	9	27	.36	10	1.4
5	10	23	.34	10	1.2
6	10	16	.33	35	0.0
7	8	16	.30	10	0.8
8	9	43	.44	10	2.3
8	10	43	.44	10	2.3
9	11	0	.02	768	0.0
9	12	0	.02	768	0.0
10	11	0	.02	768	0.0
10	12	0	.02	768	0.0
11	13	33	.40	11	0.8
11	14	29	.39	11	0.7
12	13	33	.40	11	0.8
12	23	67	.52	11	1.6
13	23	60	.49	11	1.5
14	16	27	.38	11	0.7
15	16	12	.33	11	0.3
15	21	34	.41	11	0.8
15	21	34	.41	11	0.8
15	24	36	.41	11	0.9
16	17	18	.35	11	0.4
16	19	16	.34	11	0.4
17	18	10	.32	11	0.2
17	22	73	.54	11	1.8
18	21	18	.35	11	0.4
18	21	18	.35	11	0.4
19	20	27.5	.38	11	0.7
19	20	27.5	.38	11	0.7
20	23	15	.34	11	0.4
20	23	15	.34	11	0.4
21	22	47	.45	11	1.2

Load Data

The annual peak load for this system is 2850 MW. Table C5 presents the weekly peak loads in percentage of the annual peak load. Assume week 1 is the data for the first week in January, and a winter peaking load is given for this system. Table C6 lists a daily peak load on a 7-day period cycle, in percentage of the weekly peak load value. In general, the same 7-day period peak load cycle is assumed to happen for all the year. The data in Tables C5 and C6 together with the annual peak load describes a chronological daily peak load profile of 52 × 7 = 364 days, with Monday assumed as the first day of the year. Table C7 provides weekday and weekend hourly load data for different seasons. The hourly load model of 364 × 24 = 8736 hr for the system is formed by combining the Table C5, C6 and C7 with the annual peak load value 2850 MW.

Table C5. Weekly Peak Load in Percentage of Annual Peak

Week	Peak load	Week	Peak load
1	86.2	27	75.5
2	90.0	28	81.6
3	87.8	29	80.1
4	83.4	30	88.0
5	88.0	31	72.2
6	84.1	32	77.6
7	83.2	33	80.0
8	80.6	34	72.9
9	74.0	35	72.6
10	73.7	36	70.5
11	71.5	37	78.0
12	72.7	38	69.5
13	70.4	39	72.4
14	75.0	40	72.4
15	72.1	41	74.3
16	80.0	42	74.4
17	75.4	43	80.0
18	83.7	44	88.1
19	87.0	45	88.5
20	88.0	46	90.9
21	85.6	47	94.0
22	81.1	48	89.0
23	90.0	49	94.2
24	88.7	50	97.0
25	89.6	51	100.0
26	86.1	52	95.2

Table C6. Daily Peak Load in Percentage of Weekly Peak

Day	Peak load
Monday	93
Tuesday	100
Wednesday	98
Thursday	96
Friday	94
Saturday	77
Sunday	75

Table C7. Hourly Peak Load in Percentage of Daily Peak

	Winter weeks 1-8 & 44-52		Summer weeks 18 - 30		Spring/Fall weeks 9-17 & 31-43	
Hour	Wkdy	Wknd	Wkdy	Wknd	Wkdy	Wknd
12-1 am	67	78	64	74	63	75
1-2	63	72	60	70	62	73
2-3	60	68	58	66	60	69
3-4	59	66	56	65	58	66
4-5	59	64	56	64	59	65
5-6	60	65	58	62	65	65
6-7	74	66	64	62	72	68
7-8	86	70	76	66	85	74
8-9	95	80	87	81	95	83
9-10	96	88	95	86	99	89
10-11	96	90	99	91	100	92
11-Noon	95	91	100	93	99	94
Noon-1 pm	95	90	99	93	93	91
1-2	95	88	100	92	92	90
2-3	93	87	100	91	90	90
3-4	94	87	97	91	88	86
4-5	99	91	96	92	90	85
5-6	100	100	96	94	92	88
6-7	100	99	93	95	96	92
7-8	96	97	92	95	98	100
8-9	91	94	92	100	96	97
9-10	83	92	93	93	90	95
10-11	73	87	87	88	80	90
11-12	63	81	72	80	70	85

Wkdy = Weekday, Wknd = Weekend

Generating Unit Data

Table C8 contains the generating unit ratings and reliability data. Table C9 shows operating cost data for the generating units. Power production data are also given in terms of heat rates at specific output level. Fuel costs varies due to geographical location and other factors.

Table C8. Generating Unit Reliability Data

Unit size MW	Number of units	Forced outage rate	MTTF hr	MTTR hr	Scheduled maintenance wk/yr
12	5	0.02	2940	60	2
20	4	0.10	450	50	2
50	6	0.01	1980	20	2
76	4	0.02	1960	40	3
100	3	0.04	1200	50	3
155	4	0.04	960	40	4
197	3	0.05	950	50	4
350	1	0.08	1150	100	5
400	2	0.12	1100	150	6

Table C9. Generating Unit Operating Cost Data

Size MW	Type	Fuel	Output %	Heat rate Btu/kWh	O&M cost Fixed $/kW/yr	O&M cost Variable $/MWh
12	Fossil steam	#6 oil	20	15600	10.0	0.90
			50	12900		
			80	11900		
			100	12000		
20	Combus. turbine	#2 oil	80	15000	0.30	5.00
			100	14500		
50	Hydro					
76	Fossil steam	coal	20	15600	10.0	0.90
			50	12900		
			80	11900		
			100	12000		
100	Fossil steam	#6 oil	25	13000	8.5	0.80
			55	10600		
			80	10100		
			100	10000		
155	Fossil steam	coal	35	11200	7.0	0.80
			60	10100		
			80	9800		
			100	9700		
197	Fossil steam	#6 oil	35	10750	5.0	0.70
			60	9850		
			80	9840		
			100	9600		
350	Fossil steam	coal	40	10200	4.5	0.70
			65	9600		
			80	9500		
			100	9500		
400	Nuclear steam	LWR	25	12550	5.0	0.30
			50	10825		
			80	10170		
			100	10000		

References

[1] U. S. D. o. Energy, "Final Report on the August 14, 2003 Blackout in the United States and Canada," U.S.-Canada Power System Outage Task Force, 2004.

[2] "The Hidden Cost of Fossil Fuels," Union of Concerned Scientists, [Online]. Available: http://www.ucsusa.org/clean_energy/our-energy-choices/coal-and-other-fossil-fuels/the-hidden-cost-of-fossil.html#.V0dpABUrLb0. [Accessed 14 05 2016].

[3] "Overview of Greenhouse Gases," United States Environmental Protection Agency, [Online]. Available: https://www3.epa.gov/climatechange/ghgemissions/gases/co2.html. [Accessed 3 5 2016].

[4] P. Beiter, "2014 Renewable Energy Data Book," U.S. Department of Energy's National Renewable Energy Laboratory (NREL), 2014.

[5] "Utility Scale Generation," First Solar, [Online]. Available: http://www.firstsolar.com/en/Solutions/Utility-Scale-Generation. [Accessed 5 2016].

[6] P. Gevorkian, Large scale solar power systems: construction and economics, Cambridge University Press, 2012.

[7] "Photovoltaic Power Generation System," Hitachi, [Online]. Available: http://www.hitachi.com/products/power/solar-power/outline/. [Accessed 5 2016].

[8] "Virginia Solar Project," Dominion, [Online]. Available: https://www.dom.com/corporate/what-we-do/electricity/generation/solar/virginia-solar-projects. [Accessed 5 2016].

[9] P. Kundur, Power System Stability and Control, New York: McGraw-Hill, 1994.

[10] R. D. Zimmerman, "Matpower 5.1 User's Manual," 20 3 2015. [Online]. Available: http://www.pserc.cornell.edu/matpower/manual.pdf. [Accessed 5 2015].

[11] D. Kirschen and G. Strbac, "Why Investments Do Not Prevent Blackouts," *The Electricity Journal,* vol. 17, no. 2, pp. 29-36, 2004.

[12] A. Gomez-Exposito, A. J. Conejo and C. Canizares, Electric Energy Systems: Analysis and Operation, CRC Press, 2008.

[13] "What is N-1 contingency? and how is it so important?," 4 7 2012. [Online]. Available: http://www.eng-tips.com/viewthread.cfm?qid=98869. [Accessed 5 2016].

[14] R. Billinton, "Generating capacity adequacy evaluation of small stand-alone powre systems containing solar energy," *Reliability Engineering and System Safety,* no. 91, pp. 438-443, 2006.

[15] R. Billinton and R. N. Allan, Reliability Evaluation of Power Systems, New York: Plenum Press, 1996.

[16] "Plot of the density function of several exponential distributions.," Wikipedia, 18 2 2010. [Online]. Available: https://en.wikipedia.org/wiki/File:Exponential_pdf.svg. [Accessed 5 2016].

[17] N. Ekstedt, "Reliability Evaluation of Electrical Power Systems," [Online]. Available: https://www.kth.se/social/files/55127a35f27654111f13ddc6/F2_FailureModels_NE.pdf. [Accessed 12 5 2016].

[18] "Monte Carlo Simulation," [Online]. Available: http://www.ewh.ieee.org/r6/san_francisco/pes/pes_pdf/Reliability_and_Artificial_Intelligence/Monte_Carlo_Simulation.pdf. [Accessed 12 5 2016].

[19] R. Billinton and W. Li, Reliability Assessment of Electric Power Systems Using Monte Carlo Methods, New York: Plenum Press, 1994.

[20] "National Solar Radiation Data Base," National Renewable Energy Lab, 19 1 2015. [Online]. Available: http://rredc.nrel.gov/solar/old_data/nsrdb/1991-2005/tmy3/. [Accessed 5 2016].

[21] M. Elarini, A. Othman and A. Fathy, "A New Optimization Approach for Maximizing the Photovoltaic Panel Power Based on Genetic Algorithm and Lagrange Multiplier Algorithm," *International Journal of Photoenergy,* vol. 2013, 2013.

[22] P. Wang and R. Billinton, "Time Sequential Distribution System Reliability Worth Analysis Considering Time Varying Load and Cost Models," *IEEE Transactions on Power Delivery,* vol. 14, no. 3, p. 1046, 1999.

[23] "Methods to Model and Calculate Capacity Contributions of Variable Generation for Resource Adequacy Planning," North American Electric Reliability Corporation (NERC), Princeton,NJ, 2011.

[24] D. Chung, C. Davidson, R. Fu, K. Ardani 和 R. Margolis, “U.S. Photovoltaic Prices and Cost Breakdowns: Q1 2015 Benchmarks for Residential, Commercial, and Utility-Scale Systems,” National Renewable Energy Laboratory, Golden, 2015.

[25] T. Khatib, A. Mohamed, K. Sopian and M. Mahmoud, "A New Approach for Optimal Sizing of Standalone Photovoltaic Systems," *International Journal of Photoenergy*, vol. 2012, 2012.